T · H · E
OHIO
STATE
UNIVERSITY

Analysis of the EM Scattering from Arbitrary Open-Ended Waveguide Cavities Using Axial Gaussian Beam Tracking

R.J. Burkholder, P.H. Pathak

The Ohio State University
ElectroScience Laboratory
Department of Electrical Engineering
Columbus, Ohio 43212

Final Report 719630-1
Grant No. NAG3-476
December 1988

NASA - Lewis Research Center
21000 Brokpark Road
Cleveland, OH 44135

NOTICES

When Government drawings, specifications, or other data are used for any purpose other than in connection with a definitely related Government procurement operation, the United States Government thereby incurs no responsibility nor any obligation whatsoever, and the fact that the Government may have formulated, furnished, or in any way supplied the said drawings, specifications, or other data, is not to be regarded by implication or otherwise as in any manner licensing the holder or any other person or corporation, or conveying any rights or permission to manufacture, use, or sell any patented invention that may in any way be related thereto.

50272-101

REPORT DOCUMENTATION PAGE	1. REPORT NO.	2.	3. Recipient's Accession No.

4. Title and Subtitle
Analysis of the EM Scattering from Arbitrary Open-Ended Waveguide Cavities Using Axial Gaussian Beam Tracking

5. Report Date
December 1988

6.

7. Author(s)
R.J. Burkholder, P.H. Pathak

8. Performing Org. Rept. No.
719630-1

9. Performing Organization Name and Address
The Ohio State University
ElectroScience Laboratory
1320 Kinnear Road
Columbus, OH 43212

10. Project/Task/Work Unit No.

11. Contract(C) or Grant(G) No.
(C)
(G) NAG3-476

12. Sponsoring Organization Name and Address
NASA Lewis Research Center
21000 Brookpark Road
Cleveland, OH 44135

13. Report Type/Period Covered
Final Report

14.

15. Supplementary Notes

16. Abstract (Limit: 200 words)

The EM scattering from a planar termination located inside relatively arbitrarily shaped open-ended waveguide cavities with smoothly curved interior walls is analyzed using a Gaussian Beam (GB) expansion of the incident plane wave fields in the open end. An analysis of the electromagnetic (EM) plane wave scattering by open-ended metallic waveguide cavity configurations is useful for dealing with radar cross-section (RCS) and EM penetration problems. The cavities under consideration may contain perfectly-conducting interior walls with or without a thin layer of material coating, or the walls may be characterized by an impedance boundary condition. In the present approach, the GB's are tracked only to the termination of the waveguide cavity via beam reflections from interior the waveguide cavity walls. The Gaussian beams are tracked approximately only along their beam axes; this approximation which remains valid for relatively well focussed beams assumes that an incident GB gives rise to a reflected GB with parameters related to the incident beam and the radius of curvature of the wall. It is found that this approximation breaks down for GB's which come close to grazing a convex surface and when the width of the incident beam is comparable to the radius of curvature of the surface. The expansion of the fields at the open end depend on the incidence angle only through the expansion coefficients, so the GB's need to be tracked through the waveguide cavity only once for a wide range of incidence angles. At the termination, the sum of all the GB's are integrated using a result developed from a generalized reciprocity principle, to give the fields scattered from the interior of the cavity. The rim edge at the open end of the cavity
(continued ...)

17. Document Analysis a. Descriptors

b. Identifiers/Open-Ended Terms

c. COSATI Field/Group

18. Availability Statement	19. Security Class (This Report)	21. No. of Pages
	Unclassified	72
	20. Security Class (This Page)	22. Price
	Unclassified	

(See ANSI-Z39.18) *See Instructions on Reverse* OPTIONAL FORM 272 (4-77)
Department of Commerce

Abstract (continued)
is assumed to be sharp and the external scattering from the rim is added separately using GTD. The results based on the present approach are compared with solutions based on the hybrid asymptotic modal method. The agreement is found to be very good for cavities made up of planar surfaces, and also for cavities with curved surfaces which are not too long with respect to their width. General rules of thumb for choosing the proper GB expansion parameters and length to width ratios of cavities for which the method should be accurate are presented. It is noted that the scattering from external features of the cavity (other than the open end) are not of interest here and are thus ignored. While the development is presented here for the 2-D case, it can be directly extended to treat the 3-D case in a similar fashion. Finally, based on the nature of the approximations introduced in this work, the analytical procedure here may also be viewed as a beam shooting procedure.

Contents

List of Figures

Chapter 1

Introduction

1.1 Statement of the Problem and Method of Analysis

The EM scattering from the interior of relatively arbitrary open-ended waveguide cavities with smoothly curved interior walls and with a planar interior termination is analyzed using a Gaussian Beam (GB) expansion of the incident plane wave fields at the open end. An analysis of the electromagnetic (EM) plane wave scattering by open-ended metallic waveguide cavity configurations is useful for dealing with radar cross-section (RCS) and EM penetration problems. The cavities under consideration may contain perfectly-conducting interior cavity walls with or without a thin layer of material coating, or the walls may be characterized by an impedance boundary condition. The rim edge at the open end of the cavity is assumed to be sharp for the present discussion.

In the present approach, the GB's are tracked only along their beam axes; furthermore, these beams need to travel only from the open end to the termination of the waveguide cavity via reflections from the waveguide walls. It is not necessary to track the beams from the termination back to the open end to find the fields scattered into the exterior by the termination because the use of a generalized reciprocity theorem allows one to do so with the information available from tracking the fields only one way (from the open end to the termination). The axial beam tracking approximation employed here assumes that an incident GB gives rise to a reflected GB

with parameters related to the incident beam and the radius of curvature of the wall. It is found that this approximation breaks down for GB's which come close to grazing a convex surface and when the width of the incident beam is comparable to the radius of curvature of the surface. It is important to note that the expansion of the fields at the open end depend on the incidence angle only through the expansion coefficients, and as a result the GB's need to be tracked through the given waveguide cavity only one time because the tracking of beams is made independent of the incident angle. The latter is possible because a sufficient number of beams are launched in the present approach to reproduce the field variations within the cavity in a reasonably accurate fashion for all incident angles of interest. Therefore, only the initial beam amplitudes change with the incident angle and not the beam directions. At the termination, the sum of all the GB's are then integrated using a result developed from a generalized reciprocity principle as mentioned earlier, to give the fields scattered from the interior of the cavity. The external scattering from the rim at the open end of the waveguide cavity is added separately using the geometrical theory of diffraction (GTD) and the results are compared with solutions based on the hybrid asymptotic modal method. The agreement is found to be very good for cavities made up of planar surfaces, and for cavities with curved surfaces which are not too long with respect to their width. General rules of thumb for choosing the proper GB expansion parameters and length to width ratios of cavities for which the method should be accurate are presented. It is noted that the scattering from external features of the cavity (other than the open end) are not of interest here and are thus ignored. While the development is presented here for the 2-D case, it can be directly extended to treat the 3-D case in a similar fashion. Finally, based on the nature of the approximations introduced in this work, the resulting analytical procedure developed here is referred to as the axial Gaussian beam method which may also be viewed as a beam shooting procedure.

1.2 Previous Work

A variety of waveguide cavity geometries have been analyzed in the past using various methods. The two main techniques were 1) a hybrid combination of asymptotic high frequency and modal methods, and 2) the geomet-

rical optics (GO) ray shooting method. It is noted that a rigorous analysis of the problem under consideration is possible only for a very small number of special cavity shapes, e.g., cavities formed by open-ended semi-infinite parallel plate and circular waveguides with a planar interior termination. Hence, it is necessary to resort to approximate techniques of analysis such as those indicated above. Both of these approaches involve the use of high frequency approximations.

1.2.1 Hybrid asymptotic modal method

The approach based on a hybrid combination of asymptotic and modal techniques, which is employed within the framework of the self-consistent multiple scattering method (or the generalized scattering matrix method) [1], can be applied to efficiently treat the EM scattering by open-ended cavities which can be built up by joining together waveguide sections for which the modes and their corresponding modal rays are known analytically in closed form [2,3,4]. Some examples of cavities which can be built up from different piecewise separable waveguide sections are illustrated in Figure 1.1. The high frequency asymptotic methods, e.g., the geometrical theory of diffraction (GTD) [5], and its uniform version (UTD) [6,7] as well as the equivalent current method (ECM) [7,8] and also the physical theory of diffraction (PTD) [7,9,10], are employed in this hybrid formulation to find the elements of the generalized modal scattering matrices which describe the wave reflection and transmission properties of the junctions between the different waveguide sections. The asymptotic methods provide relatively simple expressions for the elements of the generalized modal scattering matrices in contrast to the more cumbersome and far less efficient numerical modal matching or integral equation techniques.

In principle, the sizes of the generalized modal scattering matrices are infinite as the concept of ordinary scattering matrices is generalized to include both the finite number of propagating as well as the infinite number of evanescent modes in closed waveguide regions. However, in practice, the sizes of the scattering matrices are dictated by just the number of propagating modes and a few significant evanescent modes which exist within the waveguide sections on either side of the junctions. If the waveguide sections are sufficiently long then the effects of the evanescent modes can be ignored.

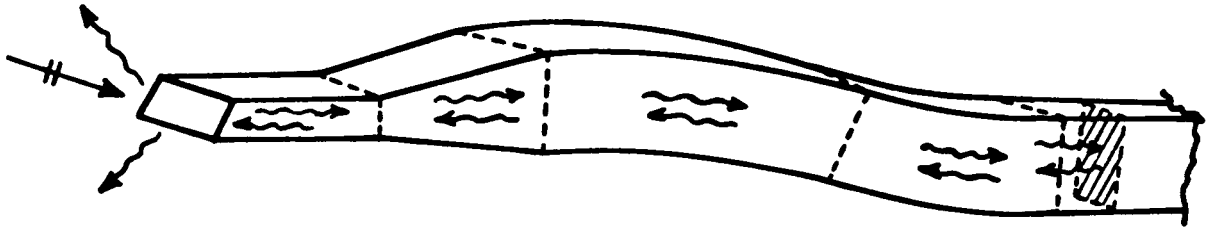

a) cavity with varying rectangular cross-section

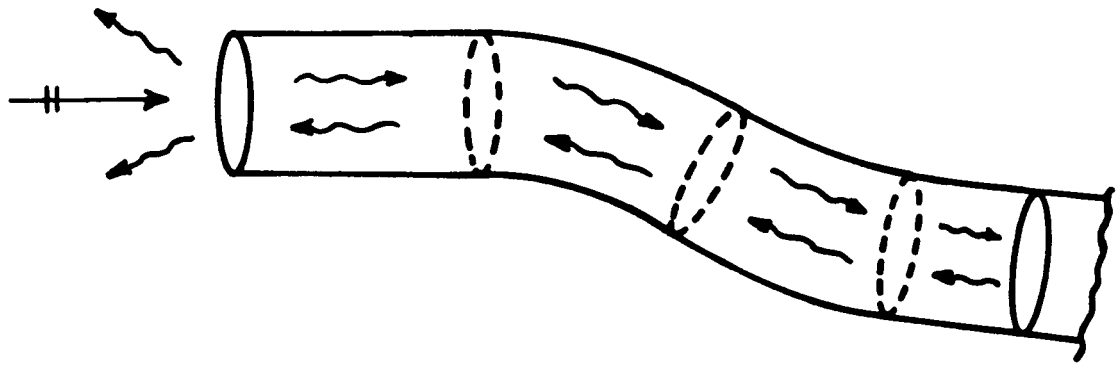

b) cavity with circular cross-section

Figure 1.1: Examples of open-ended waveguide cavities made up of piecewise uniform waveguide sections.

Finally, the field scattered by the waveguide cavity which includes the effects of all the multiple wave interactions between the various junctions is calculated in terms of the junction scattering matrices via the self-consistent multiple scattering method, or the generalized scattering matrix technique [1]; it is assumed in this calculation that the scattering (or reflection) matrix of the interior termination can also be found.

An interesting selective modal behavior which can be inferred from the hybrid asymptotic-modal analysis is that the modes most strongly coupled into (or radiated from) the open end are those whose modal ray angles are most nearly parallel to the direction of incidence (or scattering) [3,11]. The modal ray angles alluded to in the preceding statement regarding the selective modal scheme are those associated with the modes in the first waveguide section containing the open end. This selective modal scheme, which is demonstrated in Figure 1.2, can be employed to increase the efficiency of computation of the field scattered from open-ended cavities, especially at high frequencies where a large number of modes can be excited.

It is noted that a perturbation of the hybrid approach can also be employed in some relatively simple cases to efficiently but approximately take into account the effect of a thin absorber coating on the interior walls of the waveguide sections comprising the cavity [4]. On the other hand, one could also use a more rigorous procedure, but that would in general be very cumbersome both analytically and numerically.

1.2.2 Geometrical optics/aperture integration method

While the hybrid asymptotic modal procedure is useful, it is primarily suitable, as mentioned previously, to treat cavities which can be built up from piecewise separable waveguide configurations for which the modes (and modal rays) can be found analytically in closed form. On the other hand, modes in a conventional sense cannot even be defined for waveguide cavities with non-uniformly varying cross-sections. An analysis of the EM scattering by slowly varying but otherwise relatively arbitrarily shaped open-ended cavities, for which the effects of diffraction by interior walls are small, can be performed approximately via the geometrical optics (GO) ray approach used in conjunction with the aperture integration (AI) method. In this technique, the part of the incident plane wave which is intercepted by the aperture at the open end is initially divided into a sufficiently large number

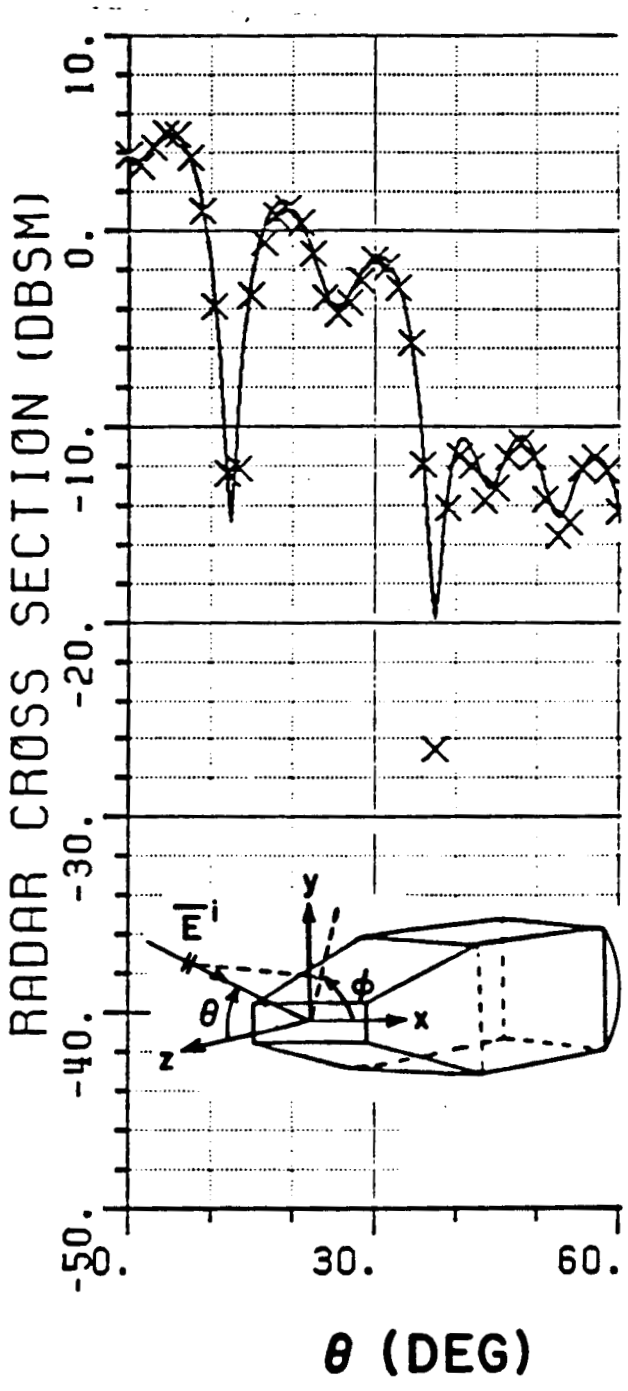

Figure 1.2: RCS pattern of a piecewise linearly tapered open-ended waveguide cavity, calculated using the hybrid asymptotic modal method, which demonstrates the selective modal scheme.

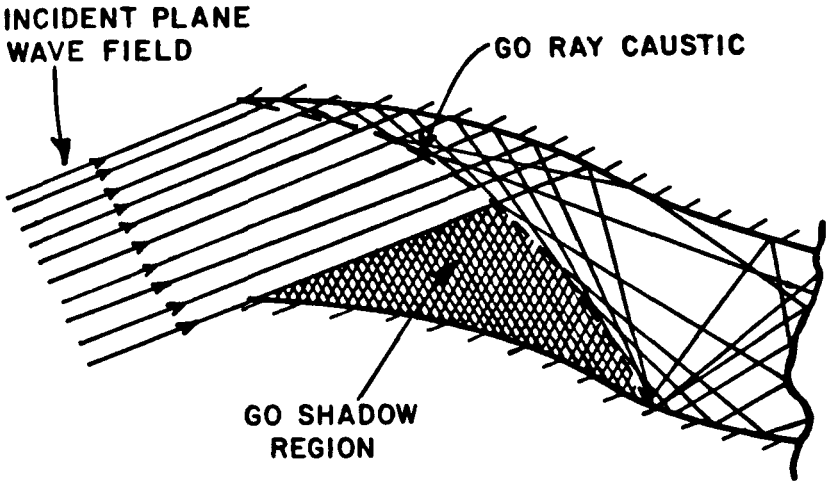

Figure 1.3: GO ray tubes launched into an open-ended cavity demonstrating a ray caustic and a shadow region.

of parallel ray tubes which are shot into the cavity as in Figure 1.3. These ray tubes (or a dense grid of rays) are then tracked via all possible cavity wall reflections to the interior termination and then back to the open end. Figure 1.4 shows one such ray tube. Each reflection off the cavity wall is calculated via the laws of ordinary GO. The polarization, divergence, phase and magnitude of each ray tube is kept track of as it is traced through the cavity.

It is noted that the ray tubes which arrive from the termination to exit from the open end generally exist only in a discrete set of directions, and hence give rise to a discontinuous field behavior. Consequently, it is necessary to evaluate the radiation integral over the equivalent sources defined by the exiting ray tubes in the aperture to obtain a continuous value for the field that comes back out of the cavity [4,13,14,15,16,17]. Figure 1.5 demonstrates several ray tubes exiting the cavity and their projections in the plane of the aperture. This combination of GO and AI procedures may be more precisely called the GO/AI technique, rather than just the GO technique. The GO/AI technique has also been referred to as the "shooting and bouncing rays" (SBR) technique in [15,16,17].

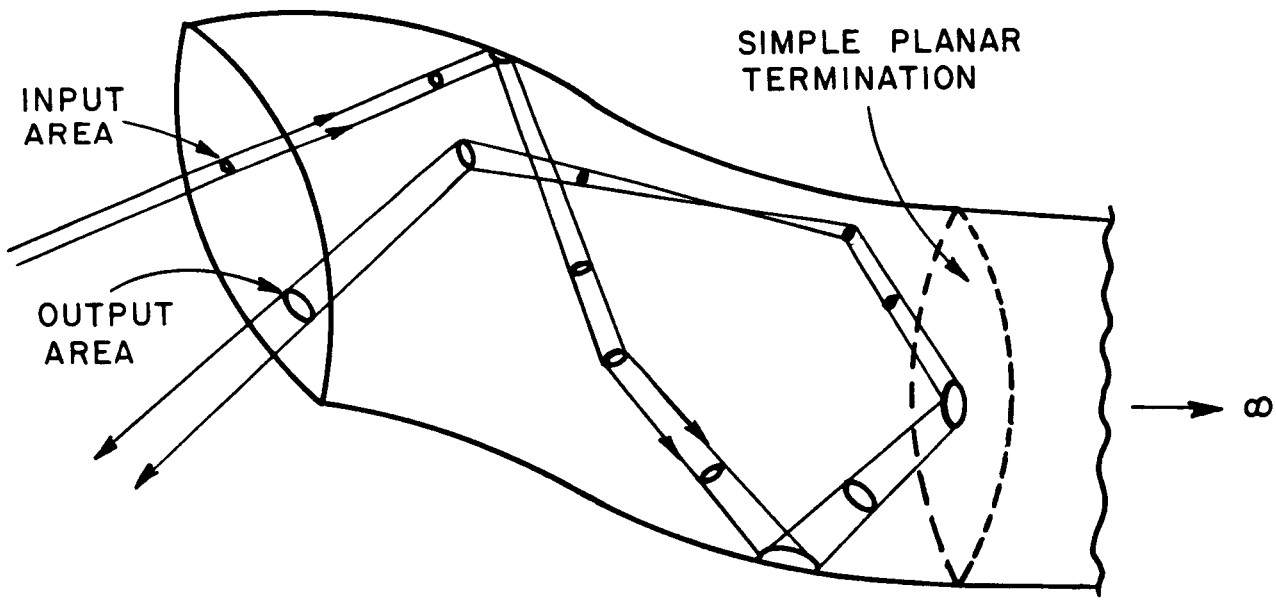

Figure 1.4: GO ray tube tracked inside a waveguide cavity until it exits through the open end.

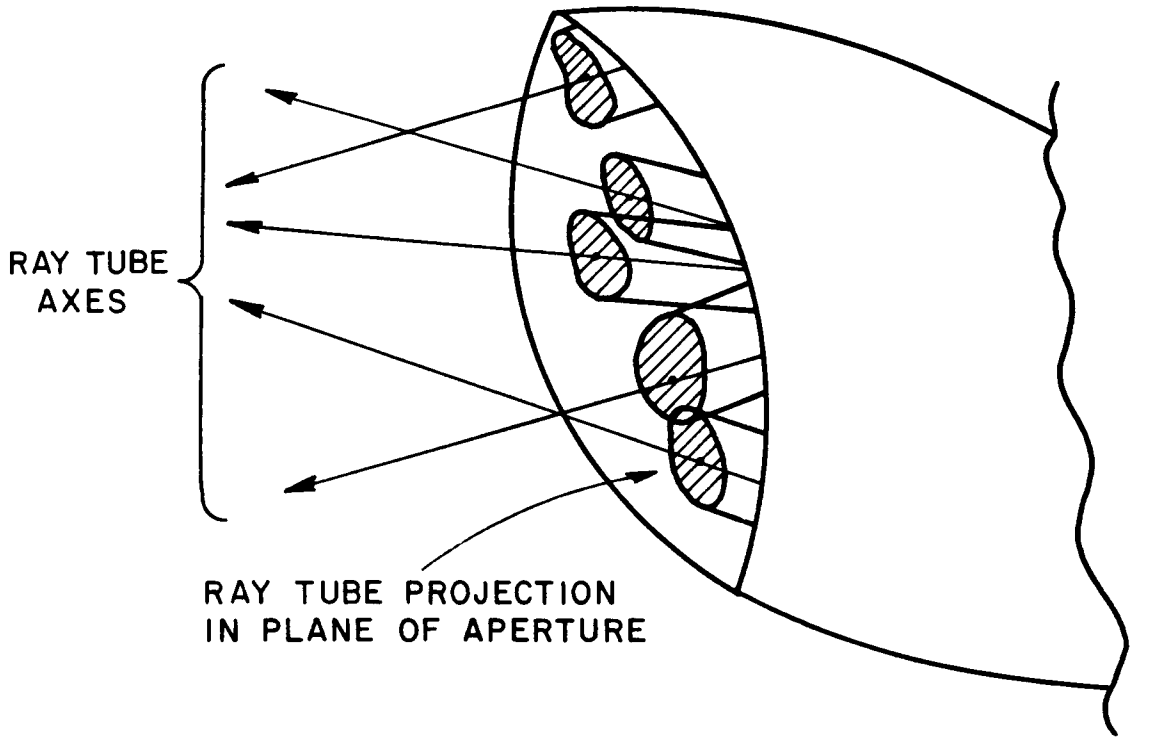

Figure 1.5: Projections of exiting ray tubes in the plane of the aperture of an open-ended cavity.

In [15], the EM scattering by a non-uniform S-shaped, three-dimensional waveguide cavity with a planar short circuit termination is analyzed. It is noted that such a conceptually simple GO/AI or SBR approach can also include the effect of absorber coating on the interior cavity walls. In general, one finds that the GO/AI (SBR) based calculations usually provide the dominant trends present in the corresponding results based on the more rigorous hybrid asymptotic-modal analysis. The details of the scattered field patterns are generally not reproduced accurately at moderately high frequencies by the GO/AI (SBR) procedure; on the other hand, this technique in general predicts the peak envelope of the RCS quite well and it tends to become increasingly more accurate at higher frequencies.

1.3 The Axial Gaussian Beam Tracking Method

It is noted that one typically requires the density of ray tubes entering the cavity aperture to be about 350 per square wavelength (in the aperture) or more for convergence in the GO/AI (SBR) approach [4,15]. Thus, at high frequencies, an extremely large number of ray tubes must be allowed to enter the cavity, and each tube must be tracked through the whole length of the waveguide cavity and back via multiple wall bounces in the GO/AI (SBR) approach. Likewise, at high frequencies, an extremely large number of modes are excited which must be included in the hybrid asymptotic-modal analysis of separable (or piecewise separable) waveguide cavity configurations. Therefore, both the GO/AI (SBR), and the hybrid approaches discussed above become cumbersome and inefficient at high frequencies.

Recently, a hybrid ray-mode analysis, which is more efficient than either the ray or the modal techniques used separately, has been developed in [18,19] for describing the fields coupled into large open-ended parallel plate and circular waveguides. A different approach which potentially retains the simplicity and generality of the GO approach, but which at the same time is more efficient and overcomes some of the limitations of the GO ray technique, is considered here. The latter approach, which like the GO/AI (SBR) approach is also a high frequency approach, employs spectrally narrow or well collimated Gaussian beams (GB's) to represent the fields launched from the open end into the waveguide cavity. Each Gaussian beam (GB) is then tracked approximately as a ray along the beam

axis. This GB approach, again like the GO/AI approach, is valid for slowly varying but otherwise relatively arbitrarily shaped open-ended waveguide cavities for which the effects of diffraction by the interior walls are small; furthermore, it can also account for the effects of absorber coating on the interior cavity walls. In previous related work, a single focussed beam (e.g., a laser beam) injected into a closed parallel plate or an open dielectric waveguide of infinite extent was tracked paraxially as one GB via the complex source point method [20]; also GB's have been employed to represent the far zone radiation fields of aperture antennas in free space [21]. Recently, a self-consistent procedure has been developed to arrive at a complete expansion for the aperture fields in terms of GB's for application to radome analysis [22]. Such a procedure [22] could also be used here to generate the GB's; however, the resulting angularly rotated GB's in that expansion will now have differing waist sizes and non-uniform angular spacing. However, the present use of GB's is somewhat different and novel in that all of the GB's are identical and equally space in angle when they are launched.

There appear to be some important advantages to be gained by using the GB approach over the GO/AI approach for the following reasons. The GO approximation neglects the effects of rays diffracted by the aperture edges at the open end which can enter into the waveguide cavity; these effects (in addition to the effects of interior cavity wall curvature) significantly diffuse the initially collimated GO incident field as it propagates large distances into the cavity. Furthermore, the GO field description fails at and near ray caustics; such ray caustics can occur if the GO rays undergo reflections from portions of the interior cavity walls which are concave (see Figures 1.3 and 1.4) or exhibit points of inflection. On the other hand, the field of the GB's launched from the aperture into the interior waveguide cavity region as in Figure 1.6 includes the contribution of the aperture edge diffracted fields which enter the cavity, and the GB description remains valid at ray caustics. It also appears that one needs to launch less than 25 GB's per square wavelength in the aperture to accurately represent the interior fields over a sufficient distance within the slowly varying waveguide cavity provided the aperture is large enough to launch well collimated GB's inside the cavity. Another significant advantage of the GB's which is not present in the GO/AI approach is that if the density of the GB's is appropriately increased to about 200 per square wavelength in the aperture, then the GB's become independent of the incident angle over a sufficiently large range of

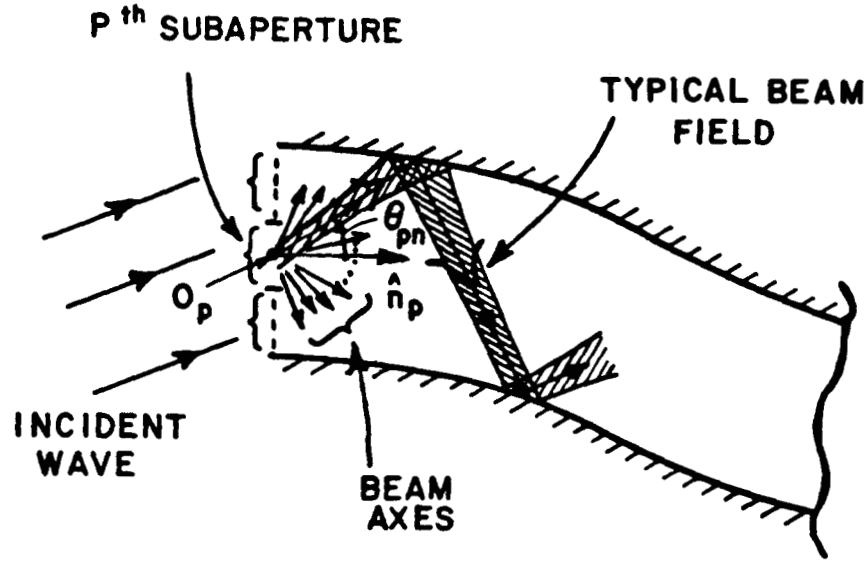

Figure 1.6: Example of one typical Gaussian beam launched into an open-ended cavity from the p^{th} subaperture.

frequencies, and therefore need to be tracked only once within the interior. In contrast, the GO rays need to be tracked each time the incident angle is changed. This advantage of the GB's comes from the fact that they can be launched as a phase-space like array which is sufficiently dense to cover the entire angular range of interest. Thus, if the expansion in terms of GB's is selected to be independent of the incident angle, then only the initial GB amplitudes change with the incident angle. Moreover, this suggests that not all GB amplitudes are significant so that one can even pre-select the most strongly excited GB's, just as in the selective modal scheme mentioned earlier [11], to once again further reduce the computational times. On the other hand, one finds that the axial (real ray) tracking of the GB's requires one to launch well focussed GB's whose spatially wide waists must fit well within the waveguide cavity. The spatially wide GB's sample a wide portion of the reflecting cavity walls and undergo distortion at each reflection thus limiting their use to waveguide cavities which are not too long compared to their width. More work needs to be done to overcome this limitation of the axial GB shooting approach.

The format of this paper is as follows. Chapter 2 will formulate the

problem and divide it up into its component parts. Chapter 3 will derive the typical Gaussian beam basis function and discuss its properties, and Chapter 4 will express the sub-aperture expansion using the GB basis function. Chapter 5 discusses how the GB's are traced inside the waveguide cavity to the termination and Chapter 6 presents some numerical results. The aspects of incidence and scattering of interest in the present work are restricted primarily to the sector $0° < \theta_i, \theta < 60°$ where the incident and scattering directions θ_i and θ, respectively, are with respect to the axis of the waveguide cavity at the open end. Furthermore, the scattering from all exterior features except by the edges at the open end of semi-infinite cavities will be excluded in the present work. Only the scattering by the edges at the open end and by the interior cavity termination are of main concern here.

The analysis in this report is predominately for the two dimensional (2-D) case. Therefore, the two possible polarizations are "soft" polarization in which the E-field is normal to the plane of the geometry, and "hard" polarization in which the H-field is normal to the geometry. Throughout the report, the letter U will be used to represent either the E-field or the H-field, depending on polarization, soft or hard, respectively. Also, U represents the scalar portion of $\vec{U}$. Finally, an $e^{j\omega t}$ time dependence for the EM fields will be assumed and suppressed in the analysis to follow.

Chapter 2

Formulation of the Axial Gaussian Beam Tracking Method

The contributions to the scattering from an open-ended waveguide cavity which are of primary interest in this work consist of the following components: the external scattering by the edges at the open end, and the internal scattering due to incident energy which is coupled to the interior of the cavity, reflected and re-radiated. All other external scattering effects from the body of which the cavity is a part of are not of interest here and are therefore not included in this analysis. Figure 2.1 shows a general two dimensional (2-D) geometry which illustrates this. The scattered field can then be written as

$$\vec{U}_{scat} = \vec{U}_{edg} + \vec{U}_{cav} \tag{2.1}$$

where $\vec{U}_{edj}$ is the edge scattering component and $\vec{U}_{cav}$ is the interior cavity scattering component.

2.1 Scattering by the Edge of the Cavity

The fields scattered by the edge at the open end of the cavity can be found easily using the Geometrical Theory of Diffraction (GTD). The scattered

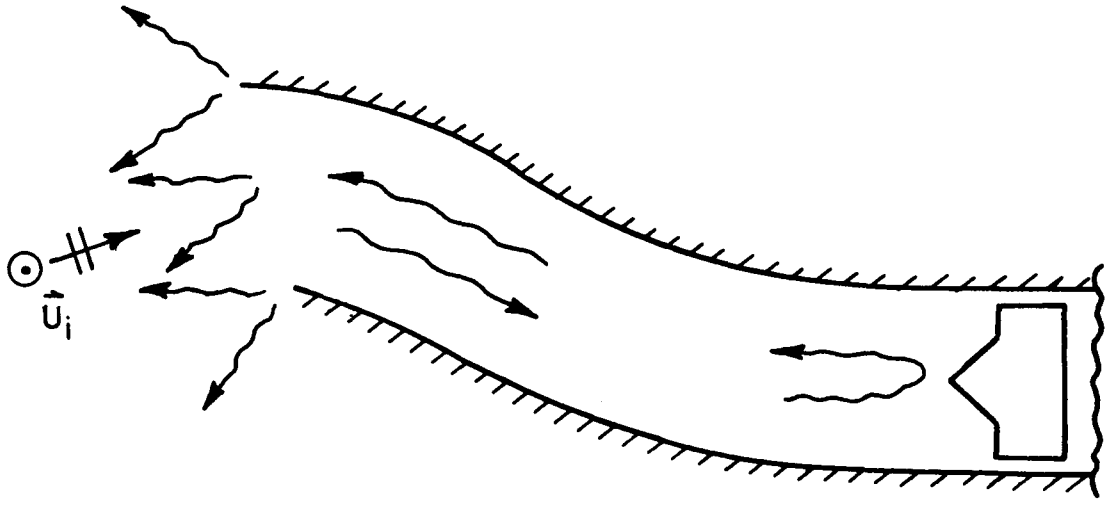

Figure 2.1: Scattering components of a 2-D open-ended waveguide cavity.

field is given to first order as (see [4])

$$\begin{aligned}\vec{U}_{edg} &= \hat{z}U_i\frac{e^{-jk\rho}}{\sqrt{\rho}}\left[D_{s,h}(\pi+\theta_d,\pi+\theta_i)e^{j\frac{1}{2}kd(\sin\theta_d+\sin\theta_i)}\right.\\ &\left.+D_{s,h}(\pi-\theta_d,\pi-\theta_i)e^{-j\frac{1}{2}kd(\sin\theta_d+\sin\theta_i)}\right] \qquad (2.2)\end{aligned}$$

where U_i is the magnitude of the incident plane wave, θ_i is the incidence angle, θ_d is the observation angle, ρ is the distance to the receiver, and d is the width of the open end, as shown in Figure 2.2. $D_{s,h}$ is the appropriate soft or hard diffraction coefficient (Keller's form, see [5]) given by

$$D_{s,h}(\phi,\phi') = \frac{\sin\left(\frac{\pi}{n}\right)}{n\sqrt{j2\pi k}}\left[\frac{1}{\cos\frac{\pi}{n}-\cos\left(\frac{\phi-\phi'}{n}\right)} \mp \frac{1}{\cos\frac{\pi}{n}-\cos\left(\frac{\phi+\phi'}{n}\right)}\right] \qquad (2.3)$$

$$n = 2-\frac{WA}{\pi} \qquad (2.4)$$

where WA is the wedge angle of the rim, as shown in Figure 2.2. The edge scattered field given by (2.2)-(2.4) includes only first order non-uniform diffraction. This first order result in (2.2) is quite adequate for large guide

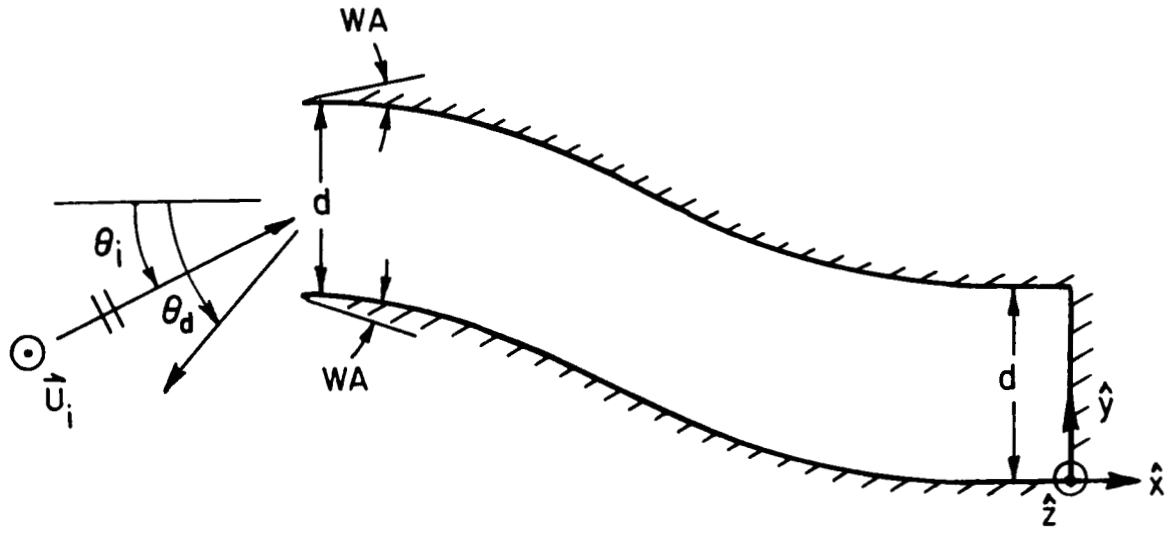

Figure 2.2: Geometry of a 2-D open-ended waveguide cavity with a planar short circuit termination.

widths d and for angles of incidence (θ_i) which are not too close to $\pm 90°$, because in these cases, the higher order (or multiple) diffraction effects are small and can be neglected.

In general, the total field scattered by a large open-ended waveguide cavity is dominated by the interior scattering, whereas, the edge scattering is almost negligible by comparison. However, if the cavity contains a large amount of loss, such as that due to interior absorber wall coatings, the edge scattering may become much more noticeable. Therefore, it is important to include this scattering mechanism in calculations, especially if there is loss present.

2.2 Scattering from the Interior of the Cavity

The contribution to the scattering from the interior of an open-ended waveguide cavity is found by coupling the plane wave field incident on the open end into the cavity and then tracking the fields via a GB expansion through

the cavity to the termination. The fields at the termination are then integrated using the reaction integral described in Appendix B and derived in [23]. Using equation (B.14) or (B.15), the cavity scattered field for a planar (short circuit) termination is then given by

$$\vec{U}_{cav} = \mp\hat{z}\frac{2}{U_i\sqrt{j8\pi k}}\frac{e^{-jk\rho}}{\sqrt{\rho}}\int_0^d\left(U_t^{ig}\frac{\partial U_e^{ig}}{\partial x}+U_e^{ig}\frac{\partial U_t^{ig}}{\partial x}\right)dy \qquad (2.5)$$

using the geometry of Figure 2.2. U_e^{ig} is the field at the termination due to a plane wave incident on the open end of the cavity from the direction of the source, and U_t^{ig} is the field at the termination due to a plane wave incident on the open end of the cavity from the direction of the receiver, both in the absence of the termination. The incident plane waves have magnitude U_i. The minus or plus sign of (2.5) is for soft or hard polarization, respectively.

The fields inside the cavity are found by first expanding the fields incident at the open end in terms of shifted and rotated Gaussian beams (GB's). Each GB in the expansion of the fields at the open end is then tracked like a ray along its beam axis, to the termination within the waveguide cavity. In order to track beams axially and maintain sufficient resolution even after successive reflections off the interior walls it is necessary to have well focussed or spectrally narrow GB's. However, such spectrally narrow GB's have wide waists. It is thus important to be able to have spectrally narrow GB's whose waists can fit easily within the waveguide cavity. Typically the initial waists of the GB's at the aperture plane should be about half the width of the original aperture. The latter can be accomplished by dividing the aperture at the open end into equally sized sub-apertures, and then expanding the fields of each sub-aperture into a superposition of rotated GB's with equal angular spacing between each rotated beam. A procedure to determine the size of the sub-apertures and the number of GB's launched per sub-aperture as well as the initial GB parameters is discussed later in Chapter 4. Figure 1.6 illustrates the sub-aperture expansion and shows one GB being tracked inside the cavity via the axial approximation. The fields at a point P_{cav} inside the cavity can then be written as

$$U_e^{ig}(P_{cav}) = \sum_{m=-M}^{M}\sum_{n=-N}^{N}A_m(\theta_i,\theta_n)B_{mn}(P_{cav}) \qquad (2.6)$$

$$U_t^{ig}(P_{cav}) = \sum_{m=-M}^{M}\sum_{n=-N}^{N}A_m(\theta_d,\theta_n)B_{mn}(P_{cav}) \qquad (2.7)$$

where $B_{mn}(P_c)$ is the field at P_c due to the Gaussian beam launched from sub-aperture m at an angle θ_n, which has been traced inside the cavity. There are $2M+1$ sub-apertures and $2N+1$ GB's per sub-aperture. $A_m(\theta_i, \theta_n)$ and $A_m(\theta_d, \theta_n)$ are the expansion coefficients for the mn^{th} GB which depend on the incidence angle θ_i and the scattering angle θ_d, respectively.

Since the expansions of (2.6) and (2.7) depend on the incidence and scattering angles only through $A_m(\theta_i, \theta_n)$ and $A_m(\theta_d, \theta_n)$, the individual beams need to be traced only once for a wide range of angles. Also, because the termination reciprocity integral of (2.5) is used, the GB's need to be tracked only to the termination and not back again to the aperture. These aspects make the GB expansion method very efficient computationally.

Next, Chapter 3 will derive the expression for B_{mn} corresponding to the GB basis function used in the expansion of (2.6) and Chapter 4 will derive the coefficients $A_m(\theta_i, \theta_n)$ of the GB expansion. Chapter 5 will then discuss how the GB's are traced along their central axis inside the waveguide cavity and Chapter 6 will present some numerical results calculated using the equations of this and subsequent chapters.

Chapter 3

Gaussian Beams as Field Basis Functions

The present Gaussian beam (GB) method uses well focused GB's to track the fields inside a waveguide cavity. This method is useful because the GB's are exact solutions to the wave equation (in paraxial regions) and therefore are well-behaved everywhere (even at caustics), and their propagation and scattering characteristics can be found using conventional techniques. Also, it has been shown by Gabor that a set of Gaussian distributions with appropriate linear phases can be used as a complete expansion for aperture fields [24,25]. The results in this report are restricted to two dimensions (2-D), however, the GB method can be extended to 3-D in a straightforward manner. In this chapter, the GB basis function which will be used in the sub-aperture expansion will be derived from a 2-D Green's function with a complex source location [26], and some of the important properties of GB basis functions will be discussed.

3.1 A Gaussian Beam as the Paraxial Field of a Point Source Located in Complex Space

A GB can be derived as the paraxial form of the 2-D Green's function when the source point is located in complex space [26]. The 2-D Green's function

is given by

$$G(r) = -\frac{j}{4}H_o^{(2)}(kr) \tag{3.1}$$

$$\approx -\frac{1}{\sqrt{j8\pi k}}\frac{e^{-jkr}}{\sqrt{r}} \; ; \; kr \gg 1 \tag{3.2}$$

$$r = \sqrt{(x-x')^2 + (z-z')^2} \tag{3.3}$$

where $H_o^{(2)}$ a Hankel function of the second kind and (x', z') and (x, z) are the source and observer locations, respectively, in the $x - z$ plane. The approximation of (3.2) is valid for $kr \gg 1$. The paraxial form of r is

$$r \approx z - z' + \frac{(x-x')^2}{2(z-z')} \tag{3.4}$$

which is valid for $(z - z')^2 \gg (x - x')^2$.

To obtain the Gaussian amplitude characteristic desired, we make the source location $(x', z') = (0, -jb)$ where b is an arbitrary positive real constant, sometimes referred to as the "beam parameter". (3.4) becomes (in the paraxial region)

$$r = z + jb + \frac{x^2}{2(z+jb)} \tag{3.5}$$

which can be re-written as

$$r = z + \frac{zx^2}{2(z^2+b^2)} - j\frac{bx^2}{2(z^2+b^2)} + jb \tag{3.6}$$

which separates the real and imaginary parts of r. Substituting this into (3.2) gives the paraxial Green's function for a complex source location as

$$G(x,z) = -\frac{e^k b}{\sqrt{j8\pi k}}\frac{1}{\sqrt{z+jb}}e^{-jkz\left(1+\frac{1}{2}\frac{x^2}{z^2+b^2}\right)}e^{-\frac{1}{2}kb\frac{x^2}{z^2+b^2}} \tag{3.7}$$

which has the familiar quadratic phase of a cylindrically spreading wave, paraxial with respect to the z-axis, along with a Gaussian amplitude distribution transverse to the direction of propagation. In other words, for a constant z, the amplitude of the beam in the transverse (x) direction is a Gaussian function centered on the z-axis. Notice also that (3.7) is not singular at $z = 0$.

3.2 The Gaussian Beam Basis Function and its Properties

The GB basis function used in this chapter has the form of (3.7) with a more convenient constant in front,

$$B(x,z) = \sqrt{\frac{jb}{z+jb}}e^{-jkz\left(1+\frac{1}{2}\frac{x^2}{z^2+b^2}\right)}e^{-\frac{1}{2}kb\frac{x^2}{z^2+b^2}} \tag{3.8}$$

chosen so that $B(0,0) = 1$. Two important parameters of the GB are the phasefront radius of curvature, $R(z)$, and the waist function, $w(z)$, which are given by

$$R(z) = \frac{1}{z}(z^2+b^2) \tag{3.9}$$

$$w(z) = \sqrt{\frac{2}{kb}(z^2+b^2)}. \tag{3.10}$$

Of these two parameters, $w(z)$ is the most often referred to because it describes the effective boundary of the beam, outside of which the amplitude of the beam is less than $1/e$ of its on-axis value (8.7 dB down). As z becomes much larger than b, (3.10) indicates that the waist function approaches a linear asymptote given by

$$w(z) = \sqrt{\frac{2}{kb}}z \tag{3.11}$$

for $z^2 \gg b^2$. Figure 3.1 shows the waist function plotted for different values of b along with its asymptote.

The beam waist width, w_o is defined as twice the minimum of the waist function:

$$\begin{aligned} w_o &= 2w(0) \\ &= 2\sqrt{\frac{2b}{k}}. \end{aligned} \tag{3.12}$$

This is a measure of the width of the beam at its narrowest point, i.e., at its waist. As Figure 3.1 shows, beams with smaller beam waists diverge faster

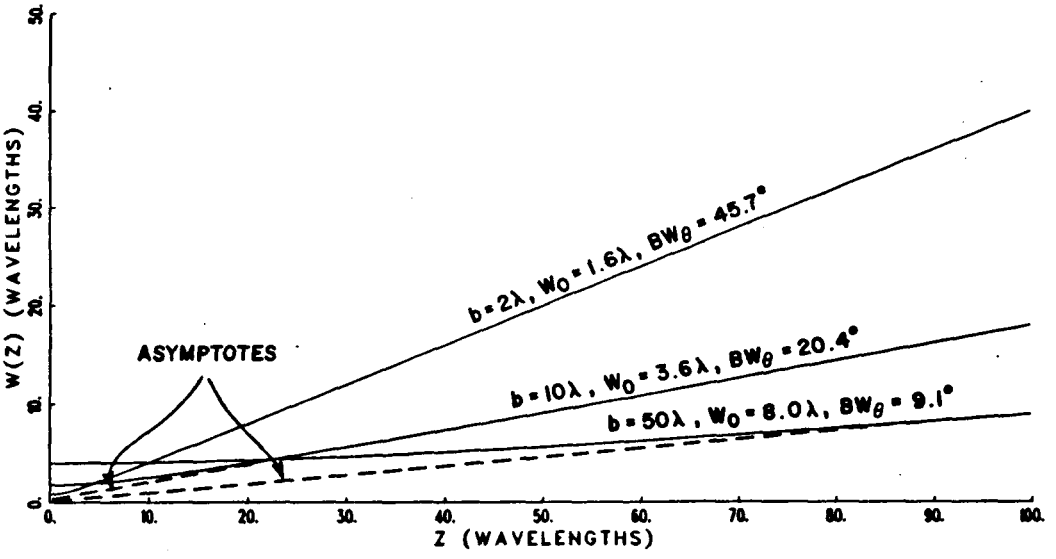

Figure 3.1: Gaussian beam waist function for 3 values of the beam parameter, b.

than beams with larger waists. However, beams with large waists may not fit inside a waveguide cavity. This is the trade-off limitation of using GB's to track the fields inside waveguides. Beams which start out small may diverge too fast and become too large to fit the waveguide after propagating a short distance. On the other hand, beams which start out with a large waist diverge slower, but they may already be too large. Therefore, this method which tracks beams axially like rays, is expected to work well only for waveguide cavities which are wide in terms of wavelength and not very long. The allowable length to width ratio will increase with frequency.

The far field form of the beam basis function (3.8) is also of interest mainly so that GB's can be matched to the far field pattern of an aperture using point matching. Changing to the (ρ, θ) coordinate system, where ρ is the distance to the observer from the origin and θ is the angular displacement from the z-axis, transforms x and z to

$$x = \rho \sin\theta \tag{3.13}$$

$$z = \rho \cos\theta. \tag{3.14}$$

Substituting these into (3.8) and letting ρ approach infinity gives

$$B(\rho,\theta) = \sqrt{\frac{jb}{\rho}} e^{-jk\rho} e^{-\frac{1}{2}kb\theta^2} \tag{3.15}$$

for $|\theta| \ll \pi$. This shows that the GB basis function is also Gaussian in the angle θ in the far field. The angular beam width, BW_θ, is defined as the $1/e$ angular width of the beam in the far field:

$$BW_\theta = 2\sqrt{\frac{2}{kb}}. \tag{3.16}$$

Comparing (3.16) and (3.12) shows that for a small angular beam width, the beam parameter b is large, giving a large waist. This was discussed earlier in terms of the waist function of (3.10) and is illustrated graphically in Figure 3.1, where the angles that the asymptotes make with the z-axis correspond to half the angular beam width.

Chapter 4

Sub-Aperture Field Expansion Using Gaussian Beams

In this chapter, the fields radiating from an aperture illuminated by a plane wave will be expanded in terms of shifted and rotated Gaussian beam (GB) basis functions. Figure 4.1 shows the geometry. Numerical results will be presented to demonstrate the use of the method and its accuracy.

4.1 Formulation of the Sub-Aperture Expansion

The sub-aperture expansion method described in Appendix A is used to write the fields in the $z > 0$ half-plane as a double summation of GB's:

$$U_{GB} = \sum_{m=-M}^{M} \sum_{n=-N}^{N} A_m(\theta_i, \theta_n) B(x_{mn}, z_{mn}) \tag{4.1}$$

which is a sum over the $2M + 1$ sub-apertures and the $2N + 1$ rotated GB's of each sub-aperture. $A_m(\theta_i, \theta_n)$ is the expansion coefficient of the GB basis function $B(x_{mn}, z_{mn})$, where (x_{mn}, z_{mn}) is the coordinate system of the mn^{th} GB, as shown in Figure 4.2. x_{mn} and z_{mn} are given in terms of x, z, and θ_n by

$$x_{mn} = (x - m\Delta)\cos\theta_n - z\sin\theta_n \tag{4.2}$$

$$z_{mn} = (x - m\Delta)\sin\theta_n + z\cos\theta_n \tag{4.3}$$

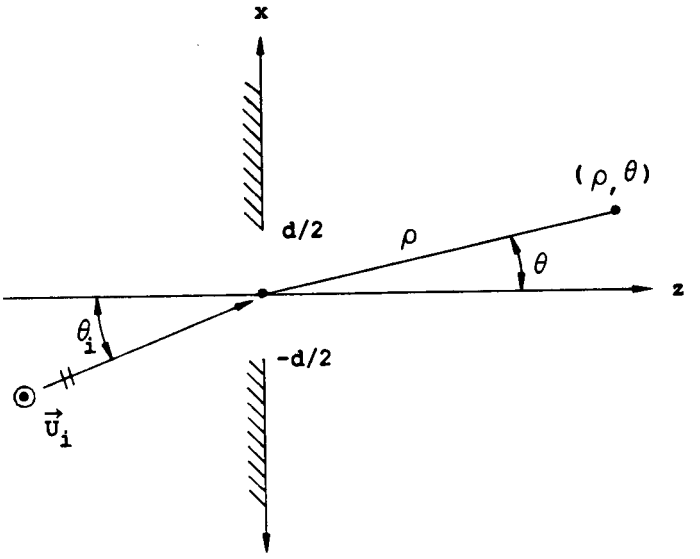

Figure 4.1: Plane wave incident on an aperture of width d.

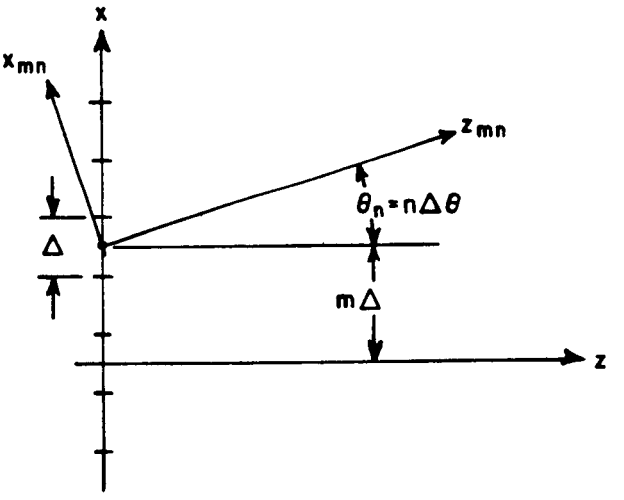

Figure 4.2: Coordinate system of the mn^{th} shifted, rotated Gaussian Beam.

where Δ is the sub-aperture width given by (A.3). The z_{mn}-axis is the beam axis of the mn^{th} GB which makes an angle of θ_n with the z-axis. The GB's are equally spaced in angle, i.e., $\theta_n = n\Delta\theta$ where $\Delta\theta$ is the angular separation of adjacent rotated beams. $B(x,z)$ is defined by (3.8).

It should be noted that the expansion of (4.1) is slightly different than the Gabor based expansion used in [25] and [21]. Gabor's expansion consists of a double summation over shifted Gaussian functions with linear phases [24]. It happens that in the paraxial region that a rotated Gaussian beam has a linear phase through its waist. Therefore, the fields of an aperture which are written as a Gabor expansion can be propagated beyond the aperture by replacing the linearly phased Gaussian functions in the aperture with shifted and rotated Gaussian beams whose waists are in the aperture. This is because the propagation characteristics of GB's are well known. However, Gabor's expansion gives rise to GB's which are not all identical and equally spaced in angle as in the expansion of (4.1) used in this report. In fact, as shown in [21], it also gives rise to evanescent type beams which die out away from the aperture; this is to be expected since the Gabor expansion is known to be complete. Gabor's expansion is a double infinite summation which must be truncated somehow to be of practical use, as investigated in [21]. In the course of the work detailed in this report, it was found that the expansion of (4.1) is more useful for the open-ended waveguide cavity application. As will be shown later, this expansion remains valid in both the near and far fields of the aperture.

To find the expansion coefficients $A_m(\theta_i,\theta_n)$, the far field pattern of the m^{th} sub-aperture illuminated by a plane wave is used. This is given by

$$U_{PO}(\rho_m,\theta_m) = 2U_o\Delta\sqrt{\frac{jk}{8\pi}}\frac{e^{-jk(\rho_m+m\Delta\sin\theta_i)}}{\sqrt{\rho_m}}\text{sinc}\left[\frac{1}{2}k\Delta(\sin\theta_m-\sin\theta_i)\right] \tag{4.4}$$

which is derived in Appendix A using the Physical Optics (PO) approximation (or equivalently, the Kirchhoff approximation). ρ_m and θ_m are the cylindrical coordinates of the m^{th} sub-aperture (see Figure A.2). U_o is the magnitude of the incident plane wave field. This far field pattern can also be written in terms of the far field form of the GB's as

$$U_{GB}(\rho_m,\theta_m) = \sum_{n=-N}^{N} A_m(\theta_i,\theta_n)B(\rho_m,\theta_m,\theta_n) \tag{4.5}$$

where

$$B(\rho_m, \theta_m, \theta_n) = \sqrt{\frac{jb}{\rho_m}} e^{-jk\rho_m} e^{-\frac{1}{2}kb(\theta_m - \theta_n)^2}. \quad (4.6)$$

The expansion coefficients $A_m(\theta_i, \theta_n)$ are found by point-matching each beam of (4.5) with the pattern (4.4) at $\theta_m = \theta_n$, i.e.,

$$A_m(\theta_i, \theta_n)\sqrt{\frac{jb}{\rho_m}} e^{-jk\rho_m} = 2CU_o\Delta\sqrt{\frac{jk}{8\pi}} \frac{e^{-jk(\rho_m + m\Delta \sin\theta_i)}}{\sqrt{\rho_m}} \operatorname{sinc}\left[\frac{1}{2}k\Delta(\sin\theta_n - \sin\theta_i)\right]. \quad (4.7)$$

Solving for $A_m(\theta_i, \theta_n)$ gives

$$A_m(\theta_i, \theta_n) = 2CU_o\Delta\sqrt{\frac{k}{8\pi b}} e^{-jkm\Delta \sin\theta_i)} \operatorname{sinc}\left[\frac{1}{2}k\Delta(\sin\theta_n - \sin\theta_i)\right]. \quad (4.8)$$

C is a constant which is introduced to account for the effects of overlapping adjacent beams. This will be discussed next, along with a way of finding the beam parameter b, in terms of the desired angular spacing of the beams, $\Delta\theta$.

Consider three adjacent GB's in the far field represented by three identical Gaussian functions of maximum amplitude C, in which each is separated by an angular rotation of $\Delta\theta$, as shown in Figure 4.3. It is desired at first to synthesize a constant function of unit amplitude in the range $4 - \frac{1}{2} < \frac{\theta}{\Delta\theta} < 4 + \frac{1}{2}$ with these three Gaussian functions. Thus, we want the superposition of the three beams in the vicinity of the central beam to be as close as possible to a constant of unity. We have two variables to adjust: the amplitude C, and the beam parameter b. By requiring that the sum of the three beams be unity at the center of the middle beam and at the point half-way between the middle beam and either of the two side beams, a system of two equations is obtained:

$$C + 2Ce^{-\frac{1}{2}kb\Delta\theta^2} = 1 \quad (4.9)$$

$$2Ce^{-\frac{1}{2}kb\left(\frac{1}{2}\Delta\theta\right)^2} = 1. \quad (4.10)$$

The constant C can be factored out and the two equations combined to give

$$1 + 2\left(e^{-\frac{1}{8}kb\Delta\theta^2}\right)^4 - 2e^{-\frac{1}{8}kb\Delta\theta^2} = 0 \quad (4.11)$$

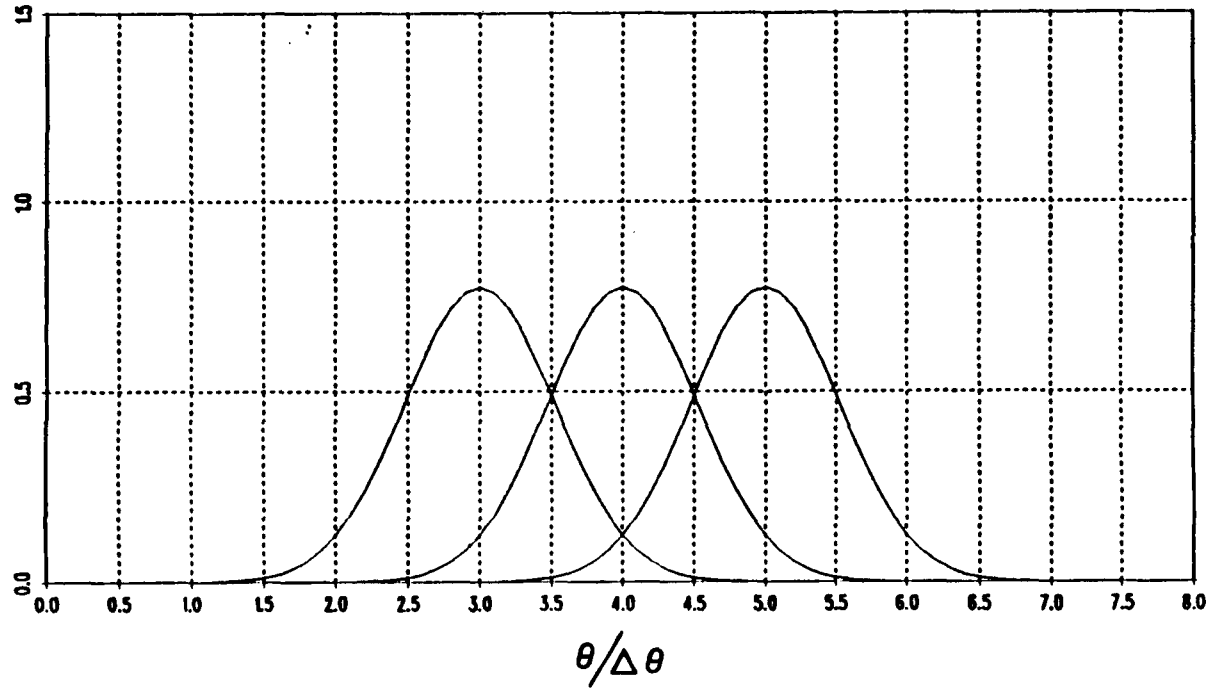

Figure 4.3: Three adjacent identical Gaussian functions separated by $\Delta\theta$.

which has only one unknown, b. Unfortunately, (4.11) has no real solution; however, it has a positive minimum at

$$b = \frac{8\log 4}{3k\Delta\theta^2}. \tag{4.12}$$

Using this value of b substituted in (4.11) gives

$$1 + 2\left(e^{-\frac{1}{8}kb\Delta\theta^2}\right)^4 - 2e^{-\frac{1}{8}kb\Delta\theta^2} = .055 \tag{4.13}$$

which was found to be close enough to zero for our purposes. This equation gives b in terms of $\Delta\theta$, either of which can be chosen to best fit the given sub-aperture size. For example, $\Delta\theta$ should be small enough so that the far field pattern is adequately reproduced by the GB expansion. This is achieved by requiring that there are at least three or four GB's per lobe of the far field pattern. However, for a small sub-aperture size the lobes might be quite large, so a larger number of narrower GB's may be desirable to keep the GB's well focused and confined within the paraxial region. On the other hand, (4.12) shows that a small $\Delta\theta$ will make b large which will make the beam waist, w_o, of (3.12) large, as discussed earlier in terms of

the angular beam width, BW_θ. In fact, the angular beam width can now be written in terms of the beam spacing by substituting (4.12) into (3.16):

$$\begin{aligned} BW_\theta &= \sqrt{\frac{3}{\log 4}}\Delta\theta \\ &\approx 1.471\Delta\theta \end{aligned} \tag{4.14}$$

which shows that the angular beam width is a little larger than the angular beam spacing, as might be expected because the GB's should overlap somewhat to adequately cover all space.

Substituting the value of b given by (4.12) into (4.9) and (4.10), respectively, suggests two values for C:

$$\begin{aligned} 1 + 2e^{-\frac{1}{2}kb\Delta\theta^2} &= 1.315 \\ &= 1/C \end{aligned} \tag{4.15}$$

$$\begin{aligned} 2e^{-\frac{1}{8}kb\Delta\theta^2} &= 1.260 \\ &= 1/C. \end{aligned} \tag{4.16}$$

The average of these two values was found to work best:

$$\begin{aligned} C &= \frac{1}{2}\left(\frac{1}{1.315} + \frac{1}{1.260}\right) \\ &= .7771 \end{aligned} \tag{4.17}$$

which again shows that the beams overlap a little, affecting adjacent beams. If there were very little overlapping, C would be closer to unity. Figure 4.4 shows the three Gaussian functions of Figure 4.3 and their sum using the b and C parameters derived above. It shows a function relatively close to unity in the vicinity of the middle beam.

While the C obtained in (4.17) synthesized a constant function of unit amplitude over a range $3.5 < \frac{\theta}{\Delta\theta} < 4.5$ with three GB's each of which has a peak value of C, the same value of C can be shown to also synthesize a linearly tapered function or more generally a function which is slowly varying within the range of $\Delta\theta$. This completes the discussion on beam synthesis of aperture fields using information provided by the far-zone patterns of sub-apertures comprising the original aperture but with the cavity walls absent. Thus, one knows the initial parameteres of the beams for launching them within the cavity.

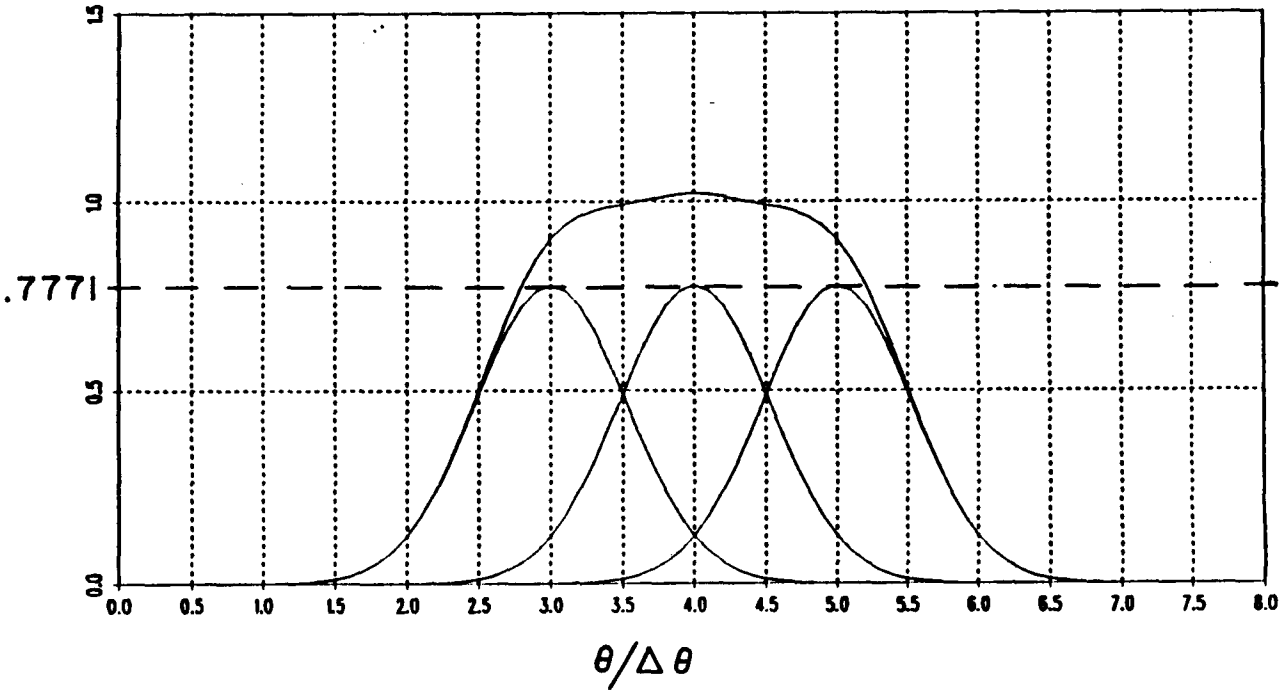

Figure 4.4: Three Gaussian functions and their sum using the derived b and C parameters.

4.2 Numerical Results

Consider the aperture geometry of Figure 4.5. It shows a 14.9 wavelength aperture illuminated by a plane wave incident at 15° and has five sub-apertures of width 2.98 wavelengths, each. Figure 4.6 shows the physical optics far field pattern of one of the sub-apertures (solid line) and its GB expansion (dotted line) which used approximately 3.5 beams per lobe of the pattern (actually, this means 3.5 beams per side lobe because the main lobe is approximately twice the width of a side lobe). Also shown are four adjacent GB's inside the main lobe which together sum up to give the middle part of the main lobe. The GB expansion can be improved in accuracy by increasing the number of beams per lobe, as shown in Figure 4.7, which is the same case as in Figure 4.6 except that 4.5 beams per lobe are used.

Figures 4.8 and 4.9 show the total aperture far field pattern found by summing the five individual sub-aperture patterns, using 3.5 and. 4.5 beams per lobe, respectively (dotted line). They both give excellent agreement with the PO result (solid line), with the 4.5 beams per lobe case being

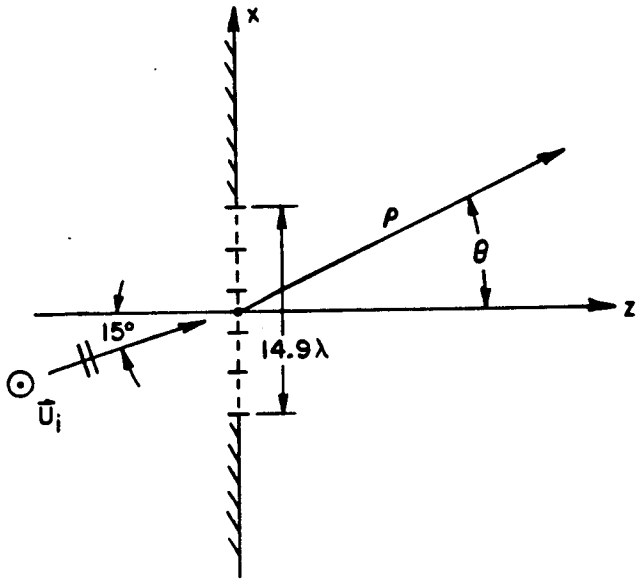

Figure 4.5: Aperture illuminated by a plane wave incident at 15° with 5 sub-apertures.

slightly more accurate than the 3.5 beams per lobe case, as expected.

Because the GB's are valid everywhere, the radiated fields can be back-tracked to the aperture and compared with the incident field in the aperture. Figures 4.10(a) and (b) show the phase and amplitude of the fields in the plane of the aperture, respectively, corresponding to the far field pattern of Figure 4.8, which used 3.5 beams per lobe. The agreement is quite good, showing that the Gaussian beam expansion of fields can be used from aperture to far field and everywhere in between. Also, because GB's propagate independently of one another, each beam can be traced individually via reflections/transmissions through complex environments, provided that there is an adequate tracing procedure available.

Notice that for the cases of Figures 4.6, 4.8 and 4.10, the width of the beam waist w_o, is 9.0 λ, which is larger than the sub-aperture width of 2.98 λ and larger than half the aperture width of 14.9 λ. This suggests a problem may arise when it comes to tracing the GB's inside a waveguide cavity of this width because the beams will start out almost as wide at the cavity aperture. This is, in fact, the main limitation of the GB tracking method when applied to open ended waveguide cavities and will be discussed in the

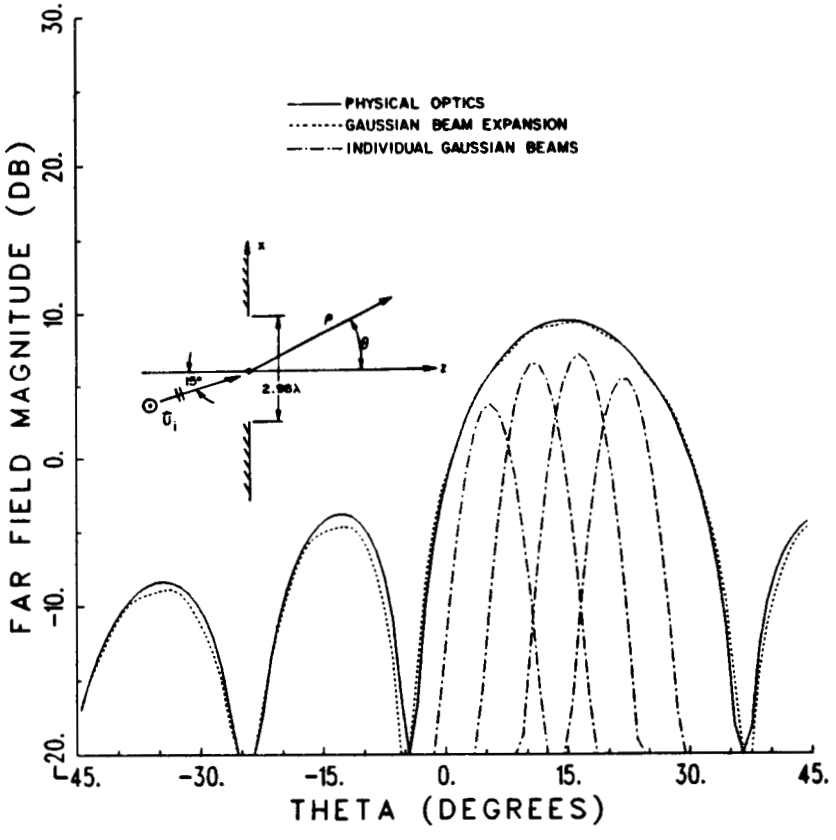

Figure 4.6: Far field pattern of a sub-aperture illuminated by a plane wave and 4 component Gaussian beams, 3.5 beams/lobe. $\Delta\theta = 5.5°$, $b = 64.0\ \lambda$, $w_o = 9.0\ \lambda$.

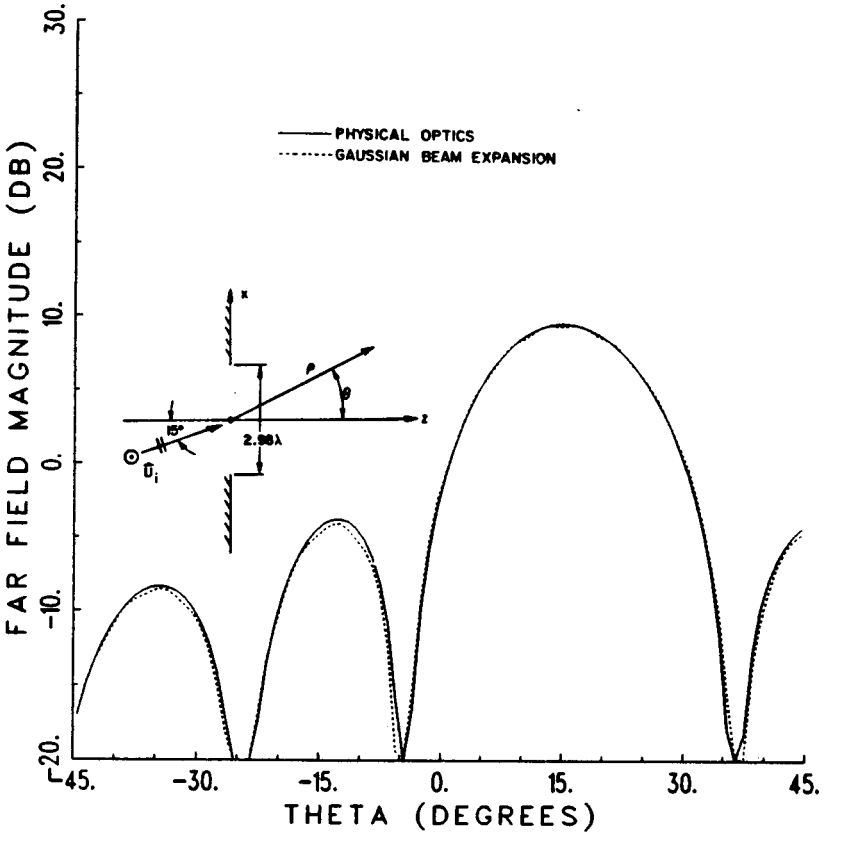

Figure 4.7: Far field pattern of a sub-aperture illuminated by a plane wave, 4.5 beams/lobe. $\Delta\theta = 4.3°$, $b = 105.8\ \lambda$, $w_o = 11.6\ \lambda$.

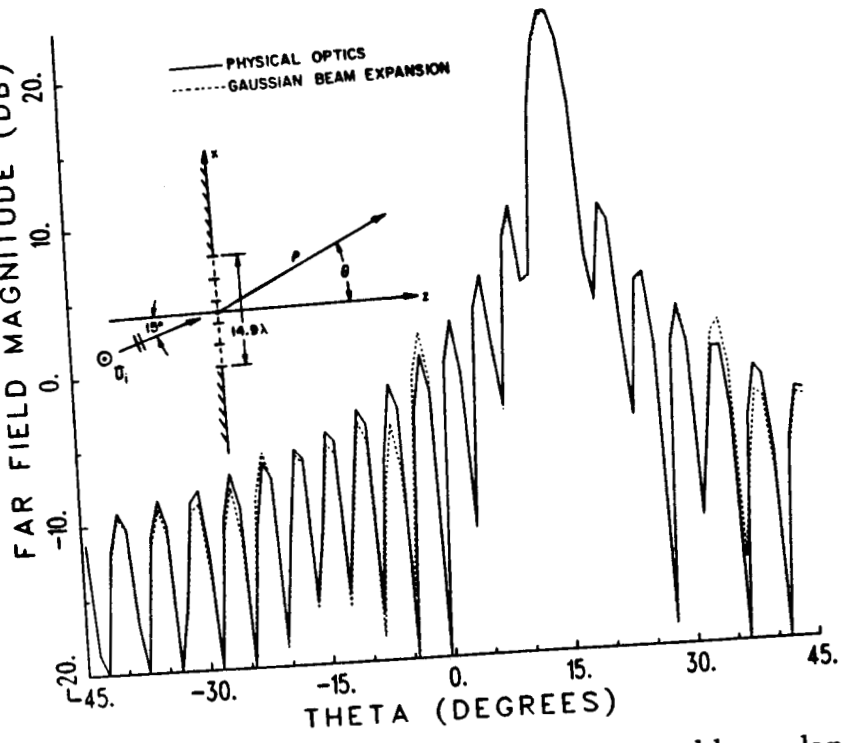

Figure 4.8: Far field pattern of an aperture illuminated by a plane wave. 5 sub-apertures, 3.5 beams/lobe, $\Delta\theta = 5.5°$, $b = 64.0\ \lambda$, $w_o = 9.0\ \lambda$.

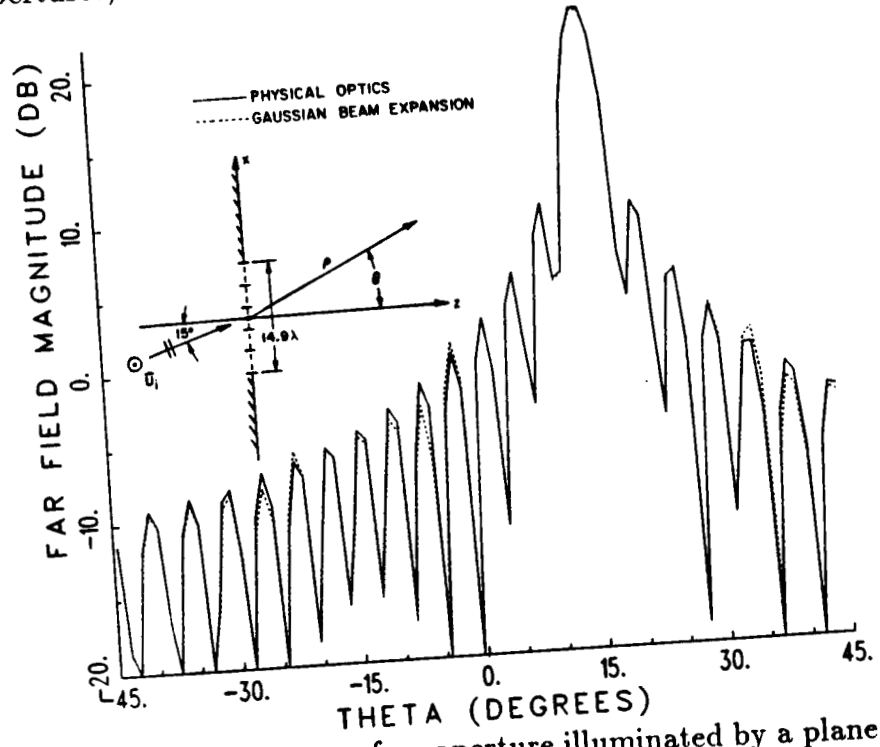

Figure 4.9: Far field pattern of an aperture illuminated by a plane wave. 5 sub-apertures, 4.5 beams/lobe, $\Delta\theta = 4.3°$, $b = 105.8\ \lambda$, $w_o = 11.6\ \lambda$.

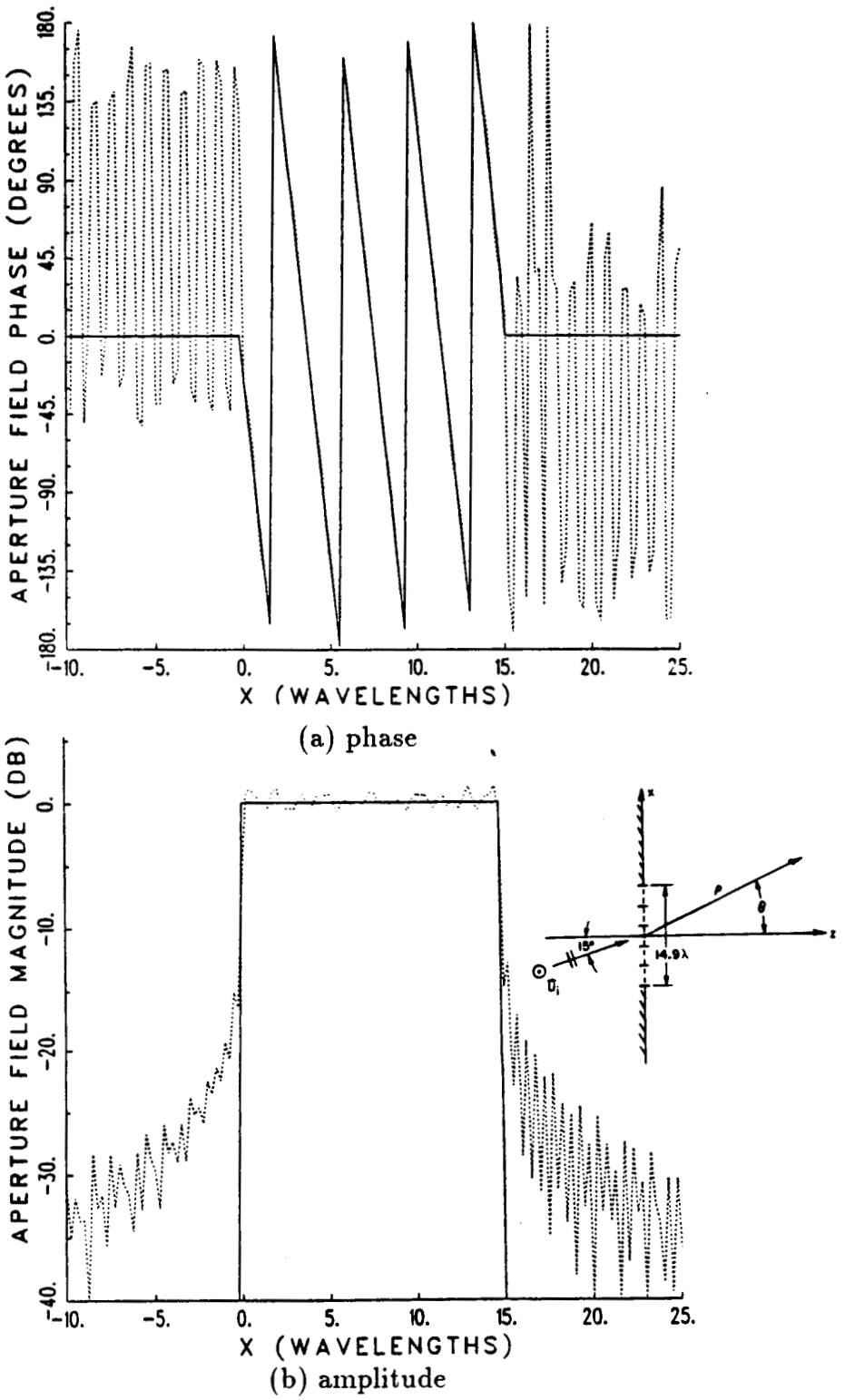

Figure 4.10: Fields in the plane of an aperture illuminated by a plane wave. 5 sub-apertures, 3.5 beams/lobe, $b = 64.0\ \lambda$, $w_o = 9.0\ \lambda$.

Chapter 5

Tracking the Gaussian Beams Axially Through the Interior of the Cavity

Once the GB's have been established in the sub-aperture expansion of the fields in the open end of the waveguide cavity, as described in Chapter 4, they must each be traced individually through the interior of the cavity to the termination. This requires insight into how the beams propagate and reflect in the presence of waveguide walls. To do this rigorously, the fields inside the cavity due to a line source must be found as accurately as possible, and then the line source can be given a location in complex space; this directly furnishes the propagation of a Gaussian beam within the same environment, as discussed in [27,28,29,30]. Recall that in Chapter 3, a line source located in complex space generates a Gaussian beam in the paraxial region along some axis. However, to find the fields due to a line source in the presence of arbitrarily shaped waveguide walls as a function of only the source and receiver location is very difficult computationally because the reflection points must be searched for numerically. When the line source is located in complex space, this search becomes an order of magnitude more difficult because the reflecting surfaces have extensions into complex space. This problem has been solved only for a few simple configurations such as reflection and transmission at a planar or curved interface between two dissimilar dielectrics [27,28], single reflection from a parabolic reflector antenna [29], and the multiple reflection of a GB inside a circular cross

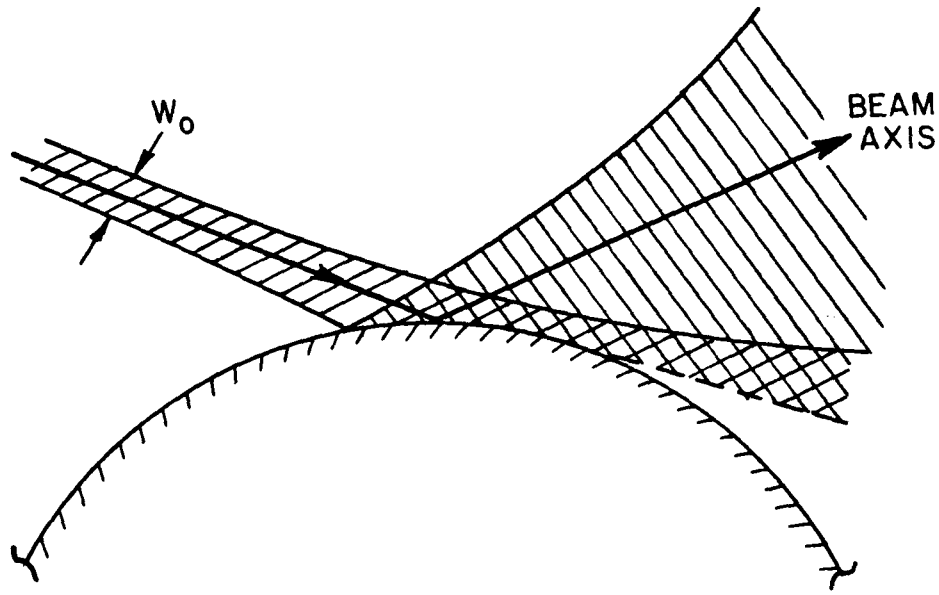

Figure 5.1: A Gaussian beam which reflects near grazing from a curved surface.

section [30].

Inside an arbitrarily shaped waveguide cavity, it is convenient to track the GB's approximately like rays by tracking only their beam axes. In other words, the GB is assumed to have most of its energy confined to a narrow region around the beam axis, and a beam which is incident on a curved reflecting surface is assumed to give rise to a new reflected beam which is also Gaussian in nature. If the parameters of this new GB can be found easily in terms of the incident beam, the GB can be traced from reflection to reflection, much like tracing a ray in the Geometrical Optics (GO) method. However, it has been shown in [28] that the reflected beam in this case may look Gaussian for many practical cases, but in general it has asymmetries present. These asymmetries arise for cases where the incident GB has a width comparable to the radius of curvature of the surface or when the incident GB grazes the surface as shown in Figure 5.1. Also, because the curvature of the interior waveguide walls gradually changes, the GB's must be kept narrow enough so that the area of the surface that they illuminate has an approximately constant radius of curvature. These limitations are not always easy to overcome, especially at lower frequencies

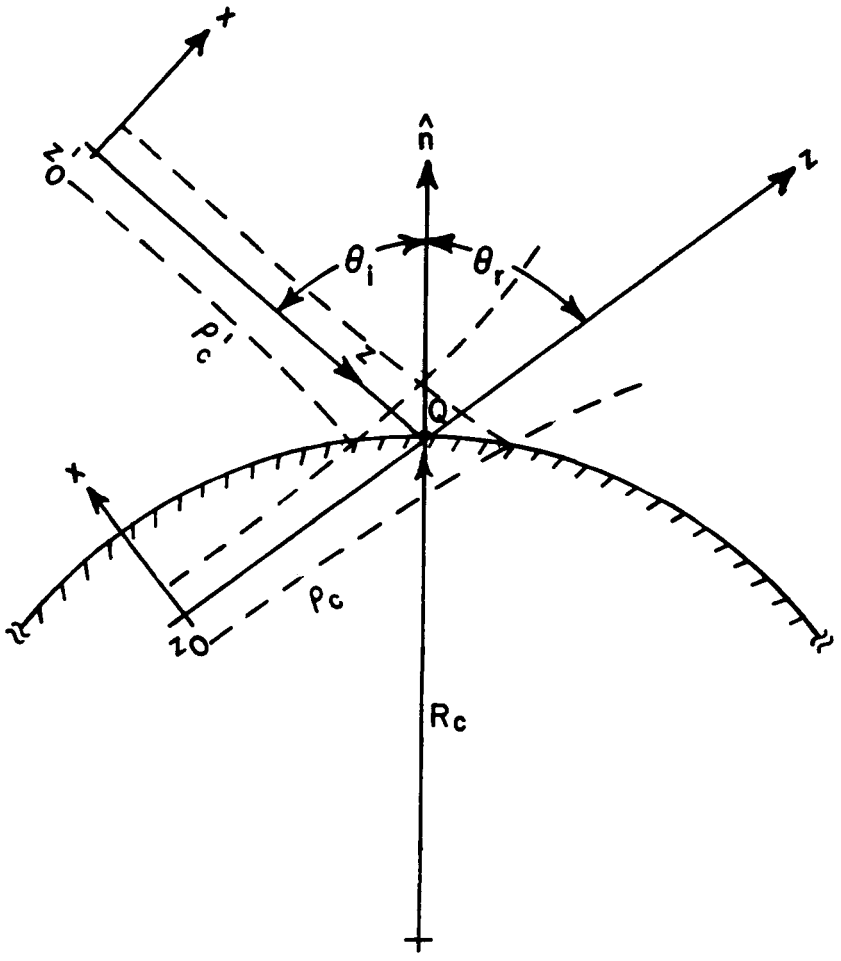

Figure 5.2: Gaussian beam reflecting off a curved surface.

and for waveguide cavities which are long compared to their width. This will be discussed further in the numerical results section.

A simple, approximate way of finding the axial reflection of a Gaussian beam from a curved surface very similarly to GO ray tracing, is derived in this chapter. As will be seen, the main difference between the reflection of the beam axis and GO reflected ray tracing is that unlike the real GO rays which have real caustic locations, the reflected beam will have complex caustic positions. This is not surprising considering that GB's can be derived from a source which is located in complex space, as described in Chapter 3. In the derivation, it is assumed that the incident GB illuminates a small area on the surface and that it does not come close to grazing incidence on the surface.

Figure 5.2 shows the geometry for a GB reflecting off a curved surface. It shows an incident beam field given by

$$U_i(x,z) = U_o'\sqrt{\frac{jb'}{z-z_o'+jb'}}e^{-jk\left[z+\frac{1}{2}\frac{(z-z_o')x^2}{(z-z_o')^2+b'^2}\right]}e^{-\frac{1}{2}\frac{kb'x^2}{(z-z_o')^2+b'^2}} \quad (5.1)$$

for $z < z_o' + \rho_c'$. In this approximation, the reflected field is assumed to be a new Gaussian beam whose axis intersects the surface at the same point as the incident beam axis. The reflected beam is given by

$$U_r(x,z) = U_o\sqrt{\frac{jb}{z-z_o+jb}}e^{-jk\left[z+\frac{1}{2}\frac{(z-z_o)x^2}{(z-z_o)^2+b^2}\right]}e^{-\frac{1}{2}\frac{kbx^2}{(z-z_o)^2+b^2}} \quad (5.2)$$

for $z > z_o' + \rho_c'$. These have the same form as the beam basis function of (3.8) but are shifted along the z-axis. The total phase propagation at any point along the beam axis is z, and x is always the coordinate transverse to the z-axis. Note that the z-axis, which is always the beam axis, changes directions after reflection. U_o, b, and z_o are the beam coefficient, beam parameter, and beam waist position along the z-axis, respectively, with the primes indicating values before reflection. ρ_c' and ρ_c are the distances from the beam waist to the point of reflection Q, before and after reflection, respectively, and R_c is the radius of curvature of the surface at Q. This derivation is also valid for concave surfaces for which R_c is negative. Here $\hat{n}$ is the unit vector normal to the surface at the point Q and θ_i and θ_r are the angles the incident and reflected beam axes make with $\hat{n}$, respectively.

The parameters of the reflected beam, U_o, b, z_o, ρ_c, and θ_r can be found in terms of the incident parameters by matching the fields on the surface in the vicinity of the reflection point of the beam axis (Q). First, matching the beams right at point Q gives

$$R(\theta_i)U_o'\sqrt{\frac{jb'}{\rho_c'+jb'}}e^{-jk(z_o'+\rho_c')} = U_o\sqrt{\frac{jb}{\rho_c+jb}}e^{-jk(z_o+\rho_c)} \quad (5.3)$$

where $R(\theta_i)$ is the reflection coefficient at Q. Inspection of this equation gives U_o and z_o as

$$U_o = R(\theta_i)U_o'\sqrt{\frac{b'(\rho_c+jb)}{b(\rho_c'+jb')}} \quad (5.4)$$

$$z_o = z_o' + \rho_c' - \rho_c. \quad (5.5)$$

The remaining parameters can be found by expanding each of the incident and reflected beam fields on the surface in a Taylor series as a function of

the displacement from point Q. Equating the constant terms of these two series gives (5.3) above. Equating the linear terms gives the relation

$$\theta_r = \theta_i \tag{5.6}$$

which is the law of reflection for a GO ray. Finally, equating the quadratic terms of the incident and reflected surface field Taylor series expansions and using the reflection law of (5.6) yields

$$\frac{1}{\rho_c + jb} = \frac{1}{\rho_c' + jb'} + \frac{2}{R_c \cos\theta_i}. \tag{5.7}$$

This is the same result as GO would give for a ray along the beam axis, except that the caustic distances are now complex ($b', b \neq 0$). Notice that ρ_c and b can be solved for separately by equating the real and imaginary parts of (5.7). This gives

$$\rho_c = R_c \cos\theta_i \frac{\rho_c'(R_c \cos\theta_i + 2\rho_c') + 2b'^2}{(R_c \cos\theta_i + 2\rho_c')^2 + 4b'^2} \tag{5.8}$$

$$b = b' \frac{(R_c \cos\theta_i)^2}{(R_c \cos\theta_i + 2\rho_c')^2 + 4b'^2}. \tag{5.9}$$

Notice from (5.9) that b is going to be smaller than b' for most cases, with the possible exception being for cases when R_c or ρ_c' is negative. The angular beam width BW_θ, given by (3.16) is inversely proportional to b. What this means is that the a GB will usually become more divergent upon reflection from a curved surface. Therefore, the farther a GB propagates inside a curved waveguide cavity, the more it will diverge and the more likely it will become too large to fit nicely inside the cavity and satisfy the restrictions of the axial beam tracing approximation. This is what limits the length to width ratio of the waveguide cavities that this method can be applied to.

The approximations used above assumed that the incident beam illuminated an area confined to the vicinity of the reflection point Q. In reality, this condition may be difficult to achieve for the two cases mentioned earlier, namely, for GB's whose beam waist function at the point of reflection $w(z_0' + \rho_c')$, is comparable to the surface radius of curvature R_c, and for beams which come close to grazing the surface. The waist function is one-half the $1/e$ width of the beam as a function of the distance along the beam

axis, measured from the beam waist (point of minimum width). It is given by

$$w(z) = \sqrt{\frac{2}{kb}(z^2 + b^2)}. \tag{5.10}$$

If the beam illuminates too large an area of the surface, such as in the two cases mentioned above, the reflected field will no longer be Gaussian in nature. In most cases it may resemble a Gaussian beam, but it will probably be asymmetric to some extent.

Once the axis of a GB has been tracked to the termination via the axial approximation, the fields of the beam in the presence of the waveguide walls in the termination plane must be found. If the beam is narrow enough and not close to the waveguide walls at the termination, as shown in Figure 5.3, the fields are simply those of the GB basis function in free space. However, if the beam crosses the termination plane near a wall, the fields of the image beam should also be included, as shown in Figure 5.4.

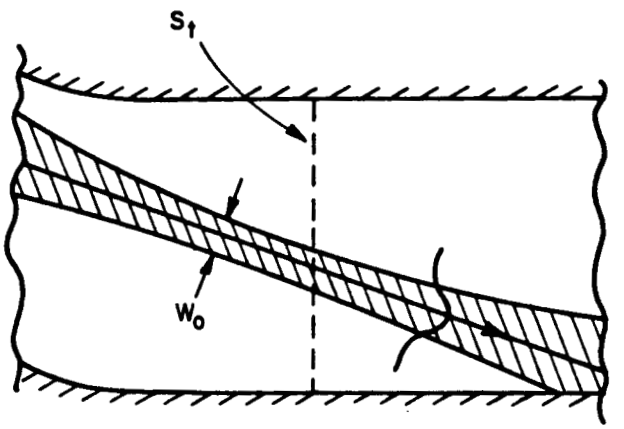

Figure 5.3: Gaussian beam crossing the plane of the termination inside a waveguide cavity, away from the walls.

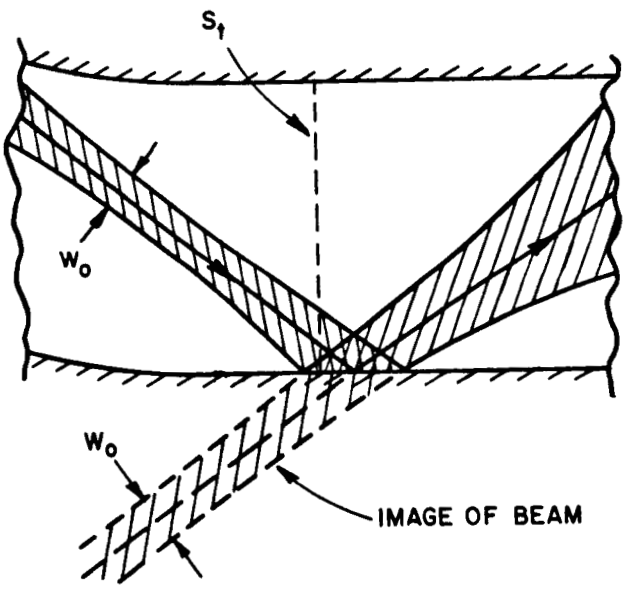

Figure 5.4: Gaussian beam crossing the plane of the termination inside a waveguide cavity, near a wall.

Chapter 6

Numerical Results

In this chapter, some numerical results are presented which illustrate the use and accuracy of the axial Gaussian beam tracking method in comparison with other methods. All of the geometries included are made up of perfectly conducting surfaces.

Figures 6.1(a) and (b) are plots of the magnitude of the fields at a cross-section inside a semi-infinite parallel plate waveguide illuminated by a plane wave, soft and hard polarization, respectively. Once again, soft polarization means the E-field is normal to the plane of the page and hard polarization means the H-field is normal to the plane of the page. For comparison, Figure 6.1 includes results found using the hybrid asymptotic high frequency modal method described in an earlier report [4]. This method is considered sufficiently accurate to be used for reference solutions. Also shown in the figures is the GO ray tracing solution which is also described in [4] for the 2-D case. As the plots show, the GO ray tracing solution is discontinuous due to shadowing effects of the GO field. The GB solution agrees nicely with the reference modal solution.

Figure 6.2 is a plot of the backscattered fields of an open-ended parallel plate waveguide cavity with a short circuit termination for the soft polarization, found using the reaction integral formulation of Chapter 2 with Gaussian beams. In this and all subsequent plots, the scattering by the rim at the open end is included in the calculations, and the wedge angle of the rim, WA, is zero. The figure also shows plots of the modal reference solution and the GO/AI ray tracing solution. The GB solution agrees nicely with the reference solution for all angles shown, while the GO/AI

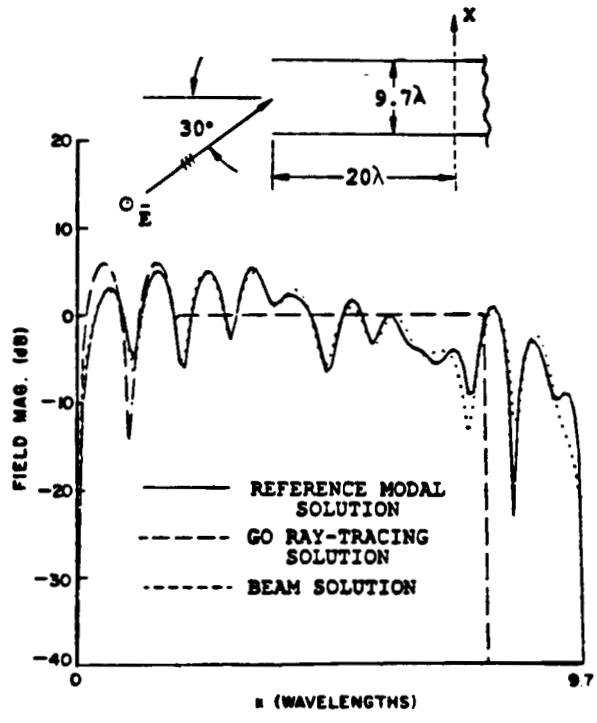

(a) soft polarization

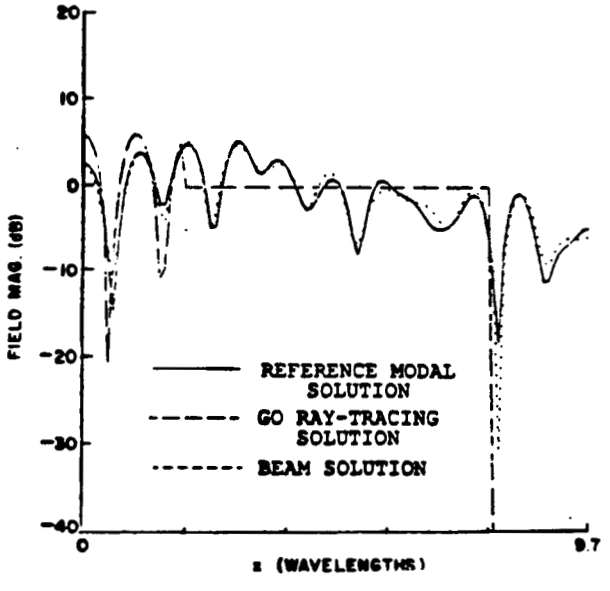

(b) hard polarization

Figure 6.1: Fields at a cross-section inside a semi-infinite parallel plate waveguide illuminated by a plane wave

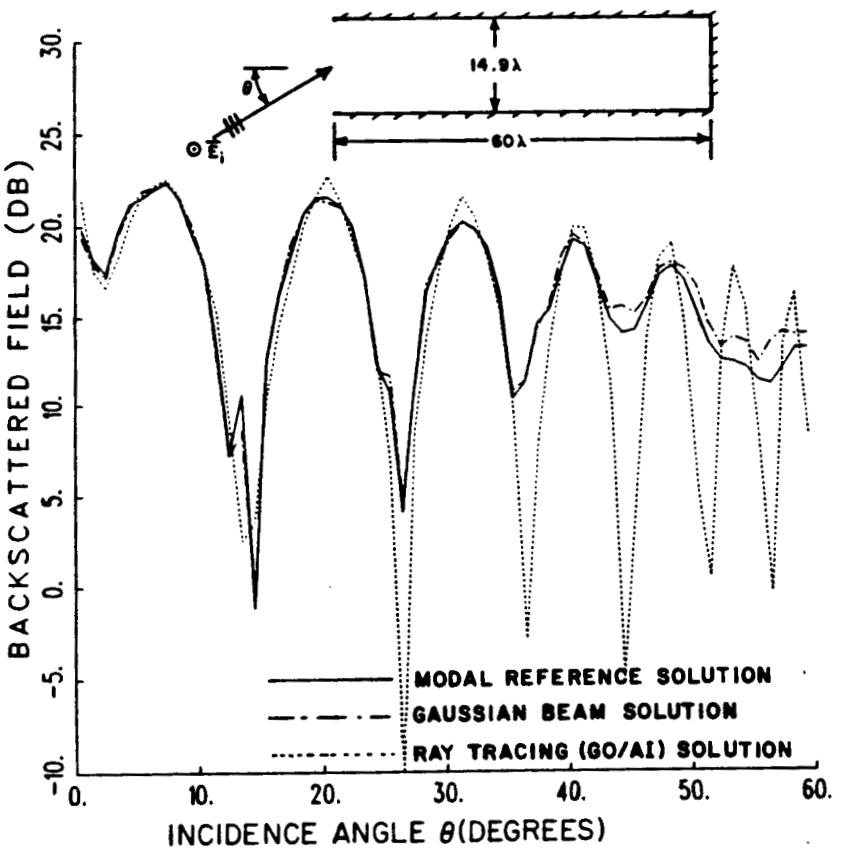

Figure 6.2: Backscatter pattern of an open-ended parallel plate waveguide cavity with a planar short circuit termination, soft polarization.

solution agrees well only for incidence angles within about 35° of of the guide axis. It is expected that the GB method should work very well for waveguide cavities with planar walls because the GB reflection from these walls is known exactly from image theory. It is the axial approximation used to find the reflection of GB's from curved walls (see Chapter 5) which introduces the most error in the GB tracing method.

Figures 6.3(a) and (b) are plots of the backscatter from an open-ended 2-D S-shaped waveguide cavity with a planar termination, soft and hard polarizations, respectively. The cavity is made up of three uniform waveguide sections, two annular guides followed by a parallel plate guide, so the hybrid modal method is used as a reference solution. Each of the sections has an axial length of 5 wavelengths making the overall axial length 15 wavelengths giving a length to width ratio (L/d) of one. The GB solution used 7 sub-apertures ($M = 3$) and an angular increment ($\Delta\theta$) of 7.69°. The beams covered an angular range of $\pm 60°$ making $N = 7$ and giving a total of 105 GB's. This choice allowed 3.5 beams per lobe (see chapter 4 for a discussion). Using (4.12) and (3.12), the beam parameter is $b = 32.7\lambda$ and the beam waist width is $w_o = 6.45\lambda$. The particular choices of sub-aperture size and angular increment were determined by trial and error. The values were used which gave the minimum number of beams which reached the termination too wide to fit in the guide. As a general rule of thumb, it is best to choose parameters which give a beam waist width w_o in the open end which is less than half the width of the waveguide and an angular beam width BW_θ which is less than 10°. Ideally, both w_o and BW_θ should be as small as possible, but since they are inversely proportional, a trade-off is necessary. For this relatively shallow cavity, the GB solution agrees very well with the modal reference solution.

Figures 6.4(a) and (b) are the same as Figures 6.3(a) and (b), respectively, except that the waveguide sections are now each 10 wavelengths long giving an overall L/d of two. Figures 6.5(a) and (b) are again the same as Figures 6.3(a) and (b), respectively, except that the waveguide sections are now each 15 wavelengths long giving an overall L/d of three. The results still agree quite well, but perhaps not as well as for the shallower $L/d = 1$ waveguide cavity.

Figures 6.6(a) and (b) are the same as Figures 6.5(a) and (b), respectively, but an additional parallel plate waveguide section of length 15 wavelengths has been inserted between the two annular sections giving an overall

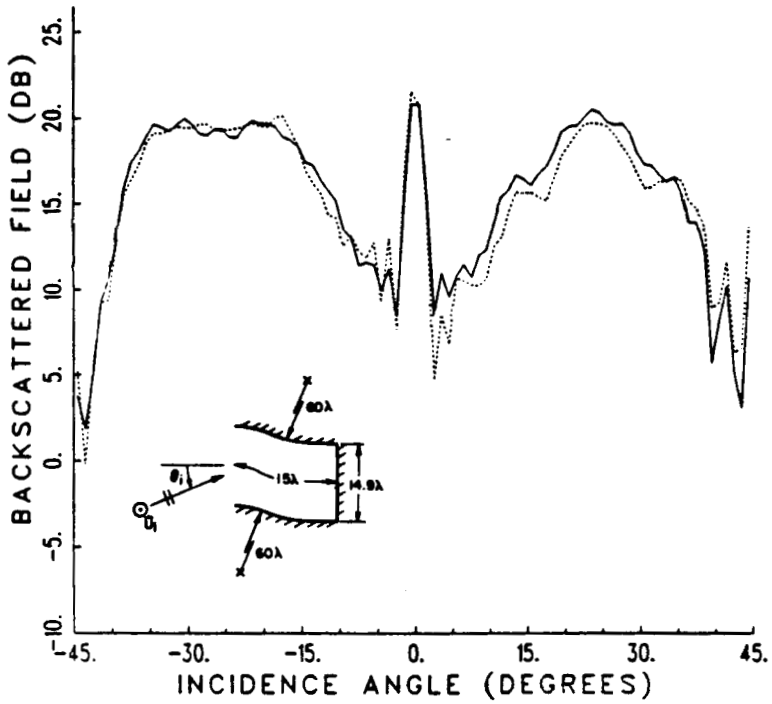

(a) soft polarization

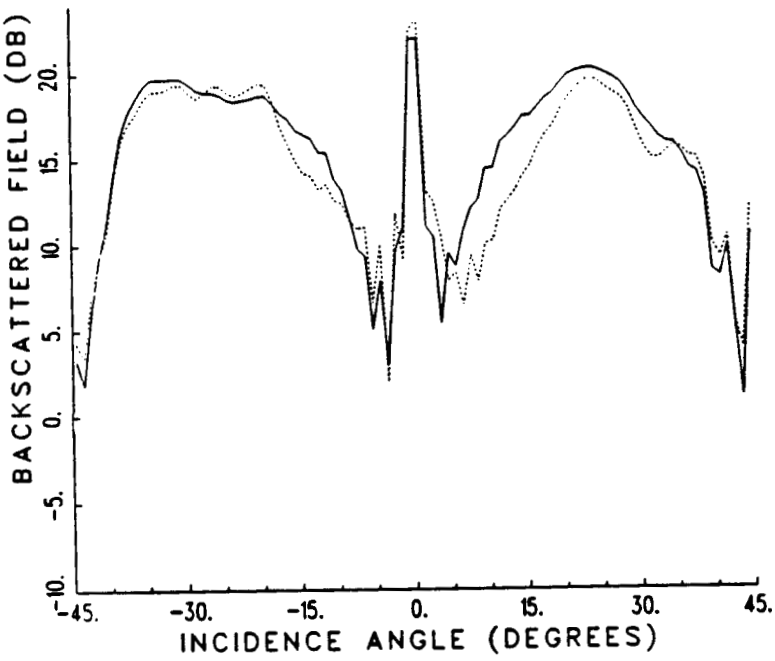

(b) hard polarization

Figure 6.3: Backscatter from an open-ended 2-D S-shaped waveguide cavity with a planar termination, $L/d = 1$, 7 sub-apertures, $\Delta\theta = 7.69°$. —— hybrid modal solution, - - - GB solution.

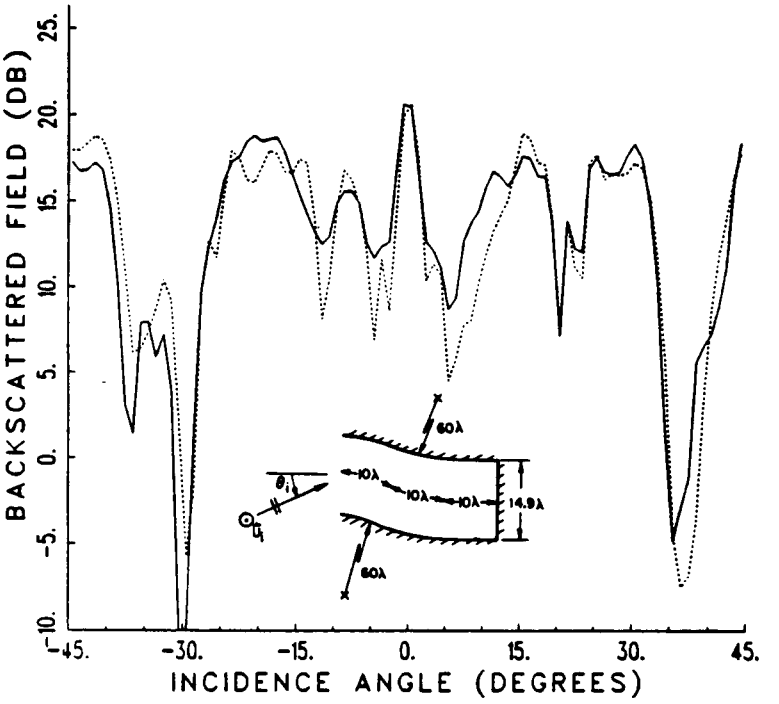

(a) soft polarization

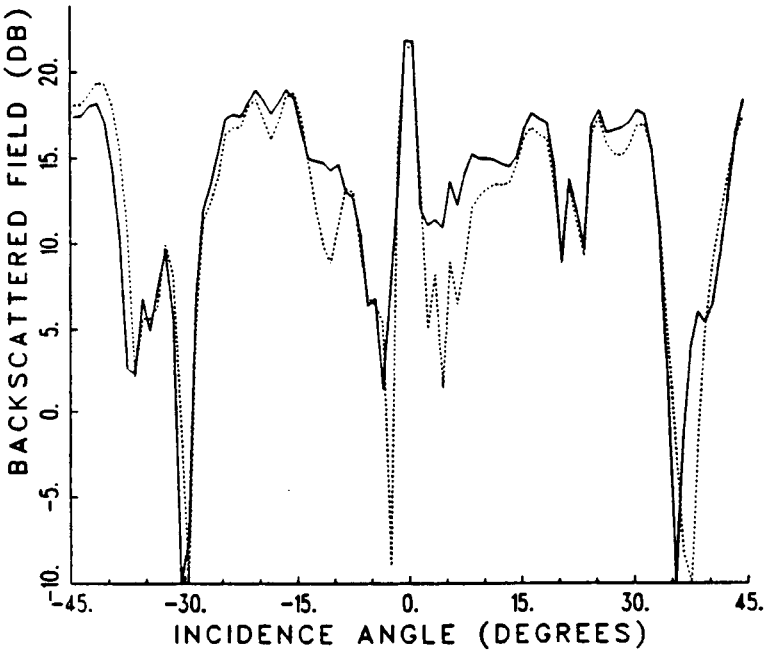

(b) hard polarization

Figure 6.4: Backscatter from an open-ended 2-D S-shaped waveguide cavity with a planar termination, $L/d = 2$, 7 sub-apertures, $\Delta\theta = 7.69°$. —— hybrid modal solution, - - - GB solution.

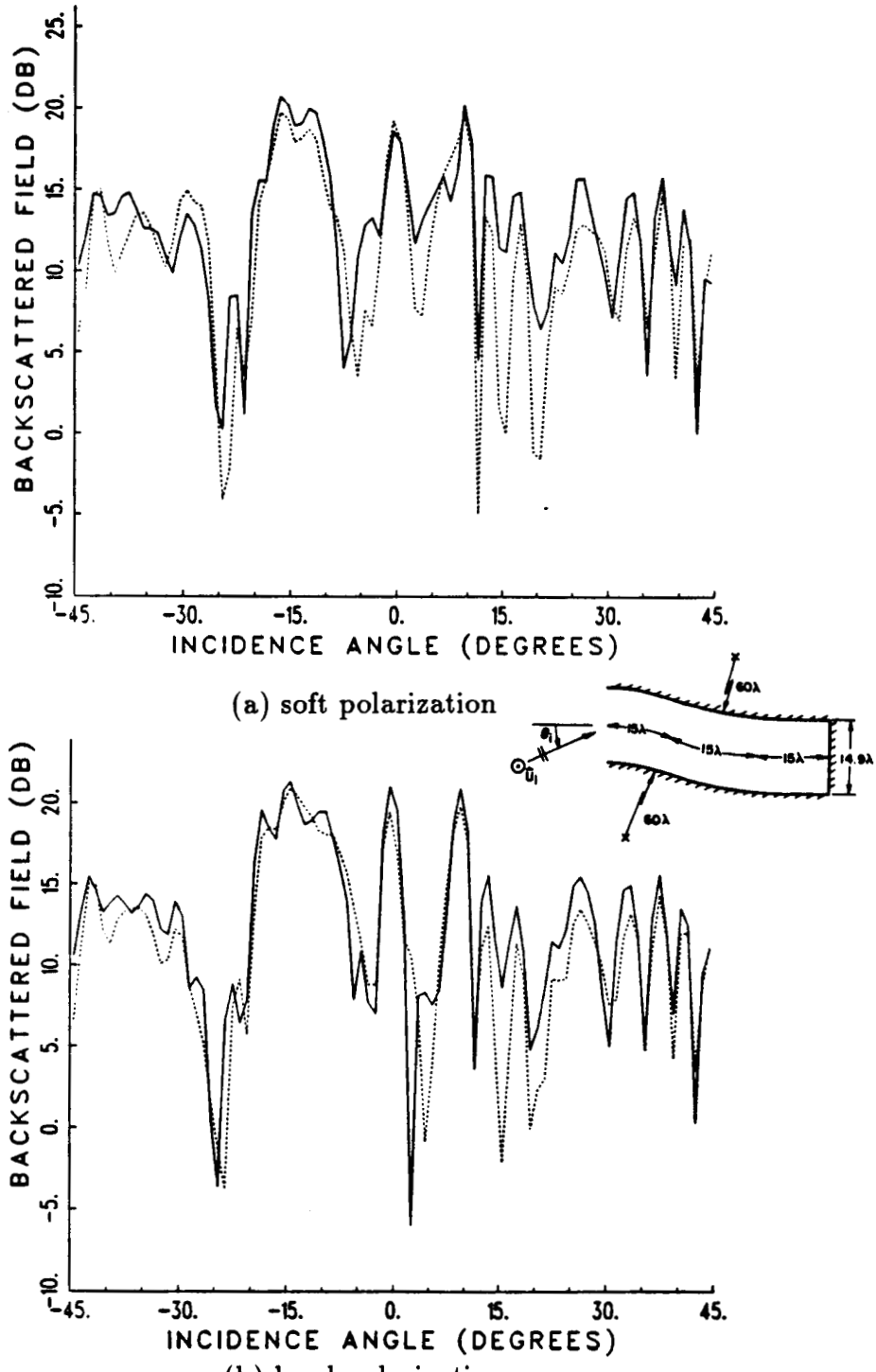

(a) soft polarization

(b) hard polarization

Figure 6.5: Backscatter from an open-ended 2-D S-shaped waveguide cavity with a planar termination, $L/d = 3$, 7 sub-apertures, $\Delta\theta = 7.69°$. —— hybrid modal solution, - - - GB solution.

L/d of four. These figures show the GB solution is getting worse for longer guide lengths. This is due to the fact that the GB's diverge and get wider the farther in they go until they are too wide to fit inside the waveguide. However, because GB's become better focussed at higher frequencies, i.e., they stay narrow over longer propagation paths, the cavities which the GB tracing method can handle are determined by frequency as well as the axial length to width (L/d) ratio. Figure 6.7 is the same as Figure 6.6(a) except the frequency is doubled. For this plot 11 sub-apertures and an angular increment of 6.04° were used. It shows a much better agreement with the modal solution than Figure 6.10 does, as expected.

It was found from experience that a general rule of thumb for applying the GB tracing method is

$$L/d \ < \ \frac{1}{4} d/\lambda \tag{6.1}$$

where d and L are the approximate waveguide cavity width and axial length, respectively and λ is the wavelength. This condition determines whether a particular cavity can be analyzed using the GB tracing method at a given frequency. The inequality of (6.1) is only an approximation and it may be found that the GB method will work well for certain waveguide cavities which do not satisfy this condition. Two specific examples of this are parallel plate and rectangular waveguide cavities for which the GB tracing method will work for much larger L/d ratios than in (6.1). This is due to the fact that the planar surfaces of these guides do not diverge the GB's any more than free space, as in image theory.

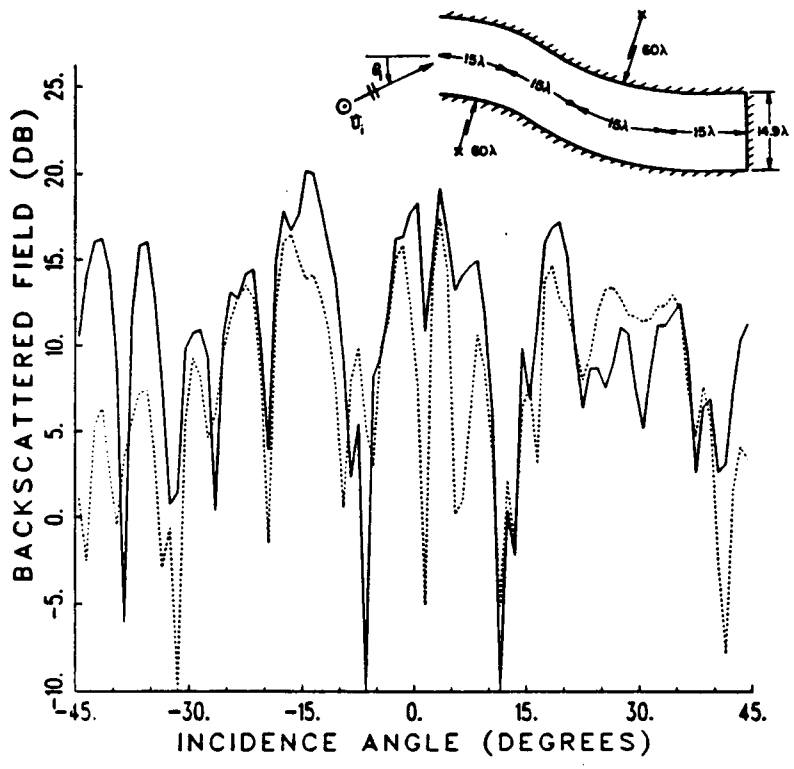

(a) soft polarization

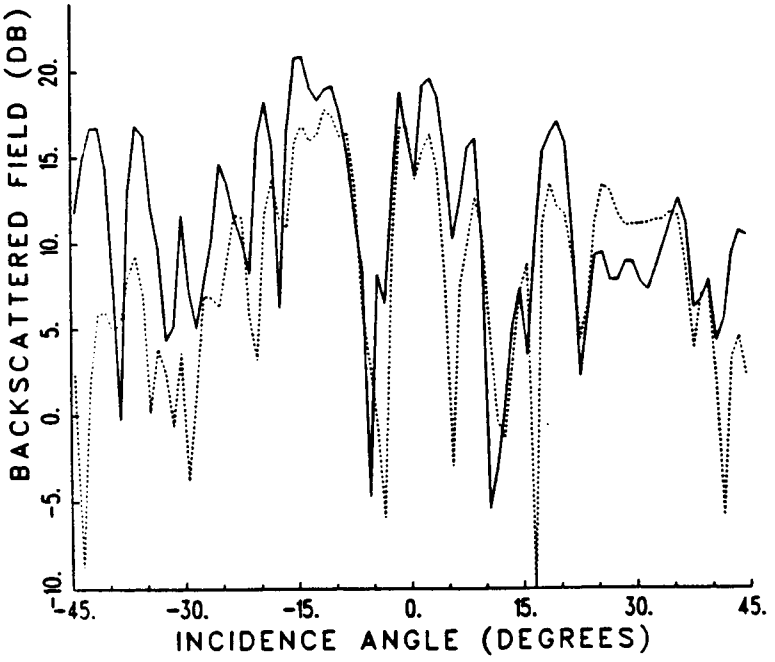

(b) hard polarization

Figure 6.6: Backscatter from an open-ended 2-D S-shaped waveguide cavity with a planar termination, $L/d = 4$, 7 sub-apertures, $\Delta\theta = 7.69°$. —— hybrid modal solution, - - - GB solution.

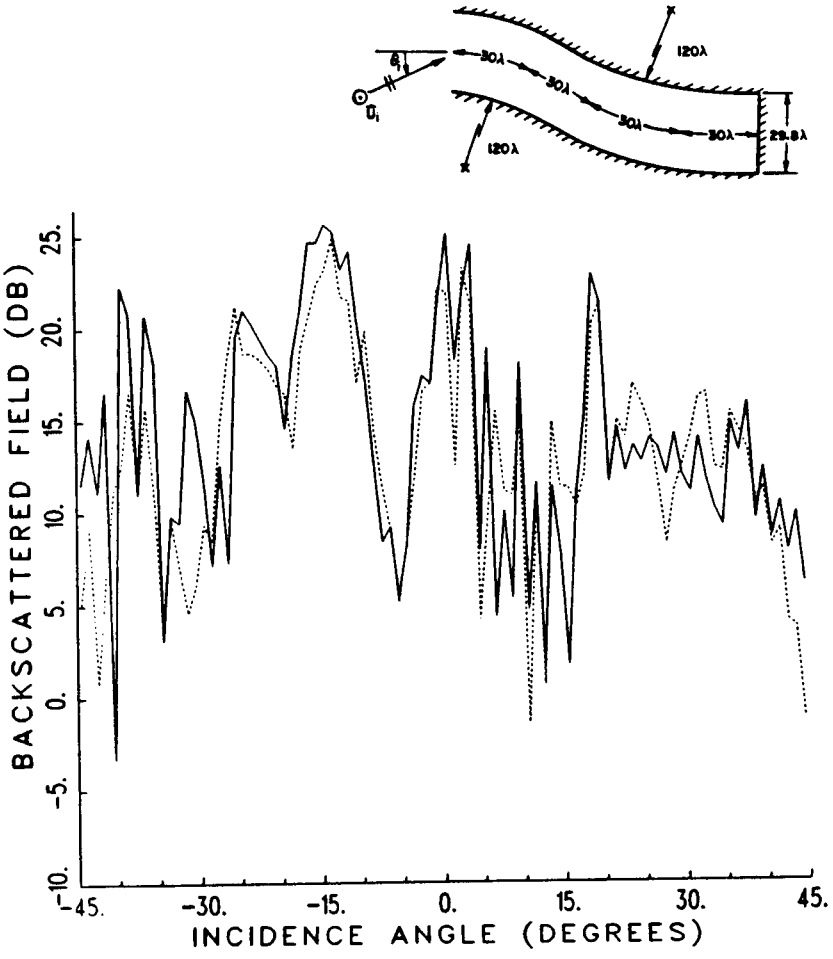

Figure 6.7: Backscatter from an open-ended 2-D S-shaped waveguide cavity with a planar termination, $L/d = 4$, soft polarization, 11 sub-apertures, $\Delta\theta = 6.04°$. —— hybrid modal solution, - - - GB solution.

Chapter 7

Conclusions

It was shown in Chapter 4 that the Gaussian beam (GB) expansion of aperture fields of a known incident field was accurate for field points everywhere from the aperture out to the far field of the aperture. If the GB's are chosen to fit within the aperture and the beam waist width in the aperture is smaller than the aperture width, the GB's can be traced from the aperture via reflections and transmission through complex environments, provided the propagation characteristics of the beams are known there. In this report the beams were traced inside arbitrary smooth waveguide cavity regions like rays along their axes from the aperture at the open end. As a rule of thumb, the beam parameters were chosen such that the beam waist width, w_o, in the aperture was smaller than one-half the aperture width, d, and the far field angular beam width, BW_θ, was less than 10°. In general, both the width of the beam with respect to the aperture and the angular beam width should be made as small as possible.

Chapter 5 showed how the GB's were traced by keeping track of successive axial reflections of the beams from the waveguide cavity walls. It was assumed that the field reflected by a curved surface with a GB incident was a new GB with parameters which were a function of the incident GB, the incidence angle and the surface radius of curvature. This axial reflection approximation was found to be accurate as long as the incident beam did not come too close to grazing the surface and the width of the beam was much smaller than the surface radius of curvature.

Once the GB's were traced to the termination of the waveguide cavity, the GB fields were integrated using the reaction integral, as formulated in

Chapter 2 and described in Appendix B, which gave the fields backscattered by the interior of the cavity. This integral did not include multiple interactions between the termination of the cavity and the open end. This contribution could have been included, but the difficulty of doing so would not have outweighed the improvement in accuracy, which would have been almost negligable. The fields backscattered by the rim at the open end of the cavity were added separately, as described in Chapter 2.

The numerical results of Chapter 6 showed excellent agreement between the GB tracking method and the hybrid modal reference solution for waveguide cavities which were not too long compared with their width. The GB's diverge as they propagate through cavities with curved walls, and eventually become too wide to fit nicely inside the waveguide region. This is what limits the length to width ration L/d. For waveguide cavities with curved walls, a general rule of thumb derived from experience was that L/d should be less than one-fourth d/λ, where d is the average waveguide width and λ is the wavelength. Therefore, the GB tracing method improves as the frequency increases or the length to width ratio decreases.

Appendix A

Sub-Aperture Field Expansion Method

The method of expanding the fields in an aperture in terms of the fields of smaller sub-apertures which make up the aperture is described in this appendix. For simplicity, the derivation is for the two dimensional (2-D) case. The extension to 3-D is straightforward and is not included in this report.

Figure A.1 shows the geometry of an aperture in the $z = 0$ plane with a known incident field $\vec{U}_i(x)$ inside the aperture. Throughout this appendix, $\vec{U}$ represents the field which is normal to the plane of the page, either electric or magnetic, depending on polarization. U means "the scalar portion of $\vec{U}$".

Using equivalent currents in the aperture and the 2-D radiation integral, the field for $z > 0$ is given by

$$U(\rho,\theta) = 2\sqrt{\frac{jk}{8\pi}}\cos\theta\int_{-\frac{d}{2}}^{\frac{d}{2}} U_i(x')\frac{e^{-jk\rho'}}{\sqrt{\rho'}}dx' \qquad \text{(A.1)}$$

where k is the free space wave number $2\pi/\lambda$, and λ is the free space wavelength. ρ' is the distance from the point in the aperture $(x', 0)$, to the field point (ρ, θ). The integral in (A.1) can be broken up into $2M + 1$ equally sized sub-apertures of width Δ:

$$\int_{-\frac{d}{2}}^{\frac{d}{2}} U_i(x')\frac{e^{-jk\rho'}}{\sqrt{\rho'}}dx' = \sum_{m=-M}^{M}\int_{(m-\frac{1}{2})\Delta}^{(m+\frac{1}{2})\Delta} U_i(x')\frac{e^{-jk\rho'}}{\sqrt{\rho'}}dx' \qquad \text{(A.2)}$$

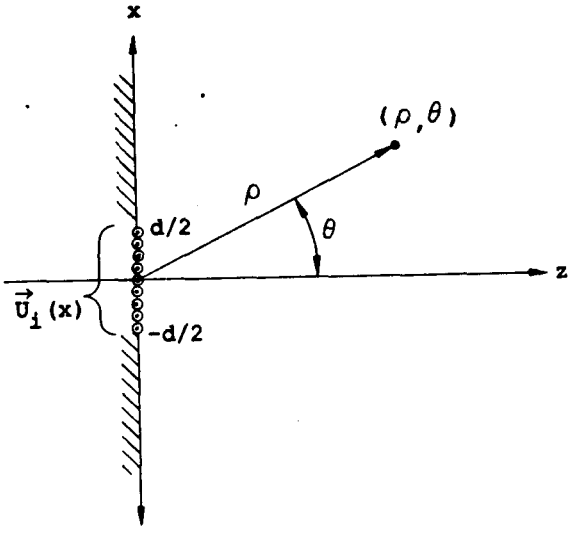

Figure A.1: Geometry of an aperture with a known incident field.

$$\Delta = \frac{d}{2M+1}. \tag{A.3}$$

Define a new variable of integration,

$$x'_m = x' - m\Delta \tag{A.4}$$

and define ρ_m and θ_m as shown in Figure A.2 for the m^{th} sub-aperture. ρ' is now given by

$$\rho' = \sqrt{\rho_m^2 + x_m'^2 - 2\rho_m x'_m \sin\theta_m}. \tag{A.5}$$

Keeping the first three terms in the Taylor series for ρ' expanded around $x'_m = 0$ gives

$$\rho' \approx \rho_m - x'_m \sin\theta_m + \frac{1}{2}\frac{x_m'^2}{\rho_m} - \frac{1}{8}\frac{(x_m'^2 - 2\rho_m x'_m \sin\theta_m)^2}{\rho_m^3}. \tag{A.6}$$

Getting rid of all terms of higher order than quadratic reduces (A.6) to

$$\rho' \approx \rho_m - x'_m \sin\theta_m + \frac{1}{2}\frac{x_m'^2}{\rho_m}\cos^2\theta_m. \tag{A.7}$$

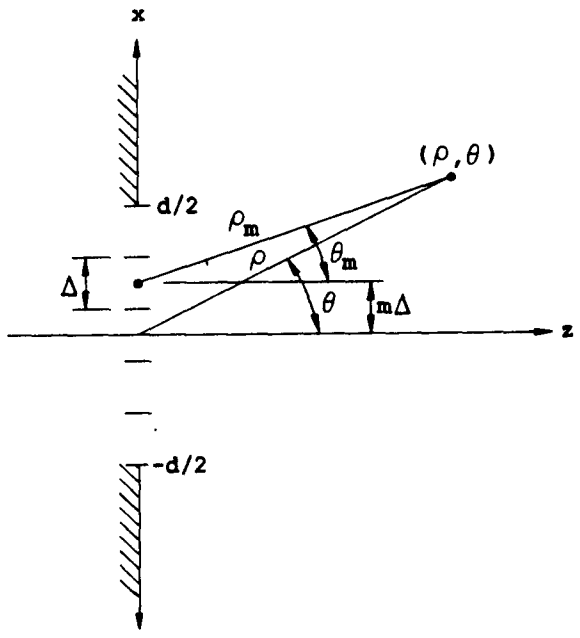

Figure A.2: Geometry of the m^{th} sub-aperture defining ρ_m and θ_m.

The quadratic term can be dropped if its phase contribution to the exponential term of (A.2) is small enough, i.e.,

$$\rho' \approx \rho_m - x'_m \sin\theta_m, \tag{A.8}$$

$$\frac{1}{2}k\frac{x'^2_m}{\rho_m}\cos^2\theta_m < \frac{\pi}{8} \tag{A.9}$$

where it is assumed that $\pi/8$ is a small enough phase to be negligible. The maximum value that x'_m can attain is $\Delta/2$. Substituting this into (A.9) for x'_m gives

$$\rho_m > 2\frac{\Delta^2}{\lambda}\cos^2\theta_m \tag{A.10}$$

which is the far field condition often encountered in aperture antenna problems. This region is plotted in Figure A.3 for a sub-aperture of width $\Delta = 2\lambda$. Equivalently, (A.10) can be written as

$$\frac{\rho_m}{\Delta} > 2\frac{\Delta}{\lambda}\cos^2\theta_m \tag{A.11}$$

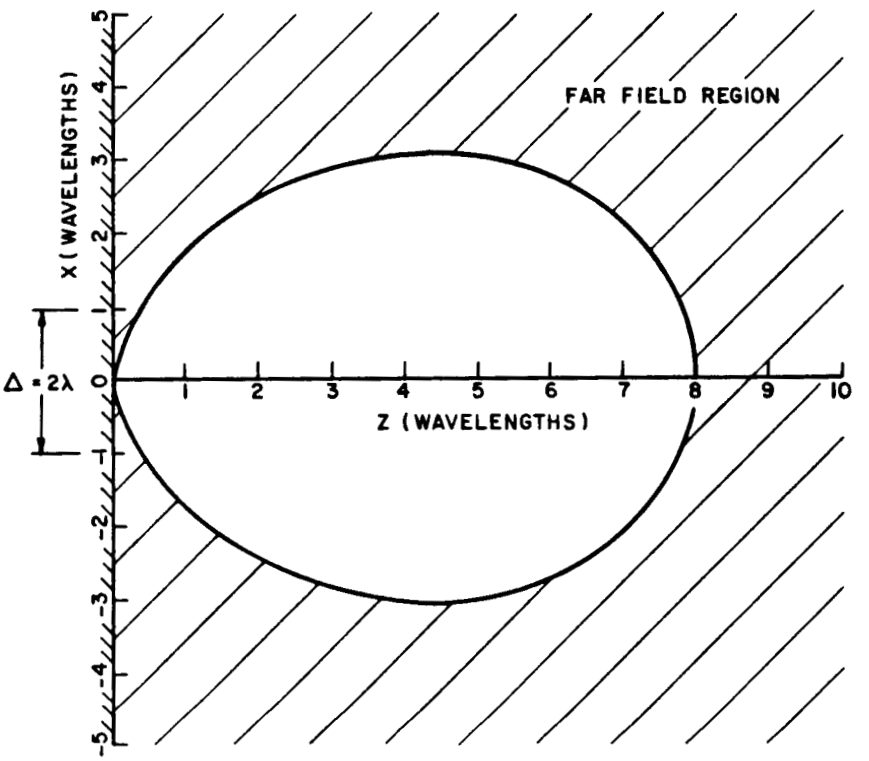

Figure A.3: Far field region of an aperture of width $\Delta = 2\lambda$.

which shows that the far field distance relative to the sub-aperture size increases as the sub-aperture gets large in terms of wavelength. This inequality is important because it determines how close the observer can be to the sub-aperture and still use the far field form of the radiation integral for a given sub-aperture size.

Substituting the far field form of ρ' (A.8) back into (A.2) along with the change of variables in (A.4) and integrating reduces (A.2) to

$$\int_{(m-\frac{1}{2})\Delta}^{(m+\frac{1}{2})\Delta} U_i(x')\frac{e^{-jk\rho'}}{\sqrt{\rho'}}dx' \approx \frac{e^{-jk\rho_m}}{\sqrt{\rho_m}}\int_{-\frac{1}{2}\Delta}^{\frac{1}{2}\Delta} U_i(x'_m + m\Delta)e^{jkx'_m \sin\theta_m}dx'_m \tag{A.12}$$

which we recognize as a simple Fourier Transform relationship. Therefore, the fields radiating from a sub-aperture look like they are due to a non-isotropic line source located in the middle of the sub-aperture with a pattern given by the Fourier Transform integral of (A.12).

Substituting this result into (A.2) and (A.2) into (A.1) gives the fields radiating from the full aperture,

$$U(\rho,\theta) = 2\sqrt{\frac{jk}{8\pi}}\cos\theta \sum_{m=-M}^{M} \frac{e^{-jk\rho_m}}{\sqrt{\rho_m}}\int_{-\frac{1}{2}\Delta}^{\frac{1}{2}\Delta} U_i(x'_m + m\Delta)e^{jkx'_m \sin\theta_m}dx'_m \tag{A.13}$$

which is valid anywhere as long as the observer is in the far field of all the sub-apertures, according to (A.10).

One advantage of using the sub-aperture expansion of (A.13) is that the far field region of each sub-aperture is much closer to the aperture plane than the far field region of the whole aperture which is given by

$$\rho > 2\frac{d^2}{\lambda}\cos^2\theta. \tag{A.14}$$

Inspection of (A.3) and (A.10) indicates that the fields of the whole aperture can be found arbitrarily close to the aperture plane using (A.13) by increasing the number of sub-apertures, $2M + 1$, appropriately. However, the main advantage of using the sub-aperture expansion technique is that the fields from any particular sub-aperture appear to be originating from a source located at the center of the sub-aperture, provided the observer

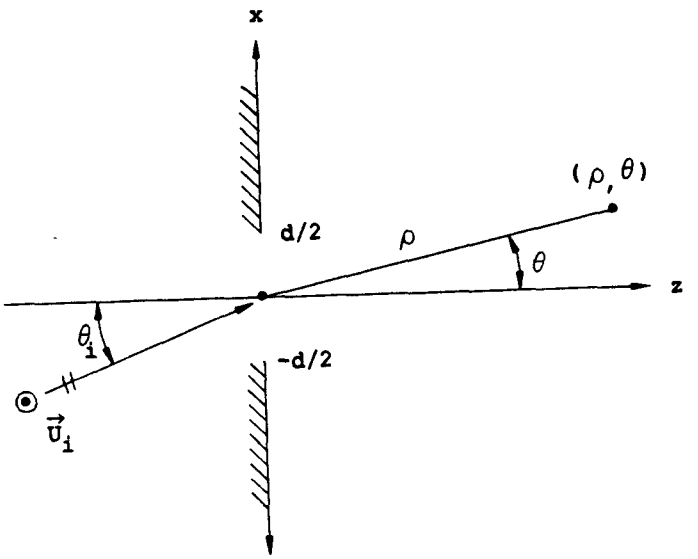

Figure A.4: Plane wave field incident on an aperture of width d in the $z = 0$ plane.

is in the far field of the sub-aperture. This allows the fields from a particular sub-aperture to be traced in the presence of obstructions, such as waveguide walls, as long as these obstructions are in the far field region of the sub-aperture, using an appropriate field tracing method. The axial Gaussian beam tracing method developed in this report is an example of such a method. However, as is seen in a Chapter 4, the Gaussian beam expansion is accurate at any distance from the aperture, not just in the far field of the sub-apertures.

As an example, let the incident field be due to a plane wave which propagates from left to right at an angle of θ_i with the z-axis, as shown in Figure A.4. This is the most common type of excitation because it represents a source located at infinity, such as a radar antenna. This is the excitation used throughout this report, although any general aperture field, $U_i(x')$, could be used as long as it is known or well approximated.

Using the Kirchhoff approximation, the incident field in the aperture is given by

$$U_i(x') = U_o e^{-jkx' \sin\theta_i}. \qquad \text{(A.15)}$$

Integrating this in (A.13), after some manipulation gives the fields radiating from the aperture as

$$U(\rho,\theta) = 2U_o\sqrt{\frac{jk}{8\pi}}\Delta\sum_{m=-M}^{M}\frac{e^{-jk(\rho_m+m\Delta\sin\theta_i)}}{\sqrt{\rho_m}}\mathrm{sinc}\left[\frac{1}{2}k\Delta(\sin\theta_m-\sin\theta_i)\right] \tag{A.16}$$

$$\mathrm{sinc}(x) = \frac{\sin x}{x}. \tag{A.17}$$

The Kirchhoff approximation used in (A.15) is very accurate for high frequencies and values of θ_i and θ which are not too close to grazing. A more accurate representation could be found using, for example, the Physical Theory of Diffraction (PTD) [9], but the improvement in accuracy would not be enough to outweigh the added complexity for realistic aperture geometries.

Appendix B

Termination Reaction Integral Formulation

In this appendix, the method of using a termination reaction integral to find the cavity scattered fields is briefly described. The derivation of the integral, which involves a reciprocity argument, can be found in [23]. The main advantage of this method is that the fields only need to be tracked from the open end of the waveguide cavity to the termination. It is not necessary to track them back from the termination to the open end. The other advantage is that this method allows the termination to be arbitrarily complex, as long as the reflection properties of the termination are known (e.g., through a modal reflection matrix or a plane wave impulse response).

B.1 General Bistatic Scattering Formulation for Three Dimensional Cavities

Figure B.1 shows an arbitrary open ended waveguide cavity illuminated by electric dipole sources $d\vec{p}_e$ at point P' and $d\vec{p}_{et}$ at point P. The scattered electric field component in the direction of $d\vec{p}_{et}$ at point P due to illumination by $d\vec{p}_e$ at point P' is given by

$$\vec{E}_e^{so}(P) \cdot d\vec{p}_{et} = \int\int_{S_a} \left(\vec{E}_t^{ig} \times \vec{H}_e^{so} - \vec{E}_e^{so} \times \vec{H}_t^{ig} \right) \cdot \hat{n} dS \qquad \text{(B.1)}$$

where S_a is a cross-sectional surface near the termination and $\hat{n}$ is the unit normal to this surface. $\vec{E}_t^{ig}$ and $\vec{H}_t^{ig}$ are the incident fields generated by

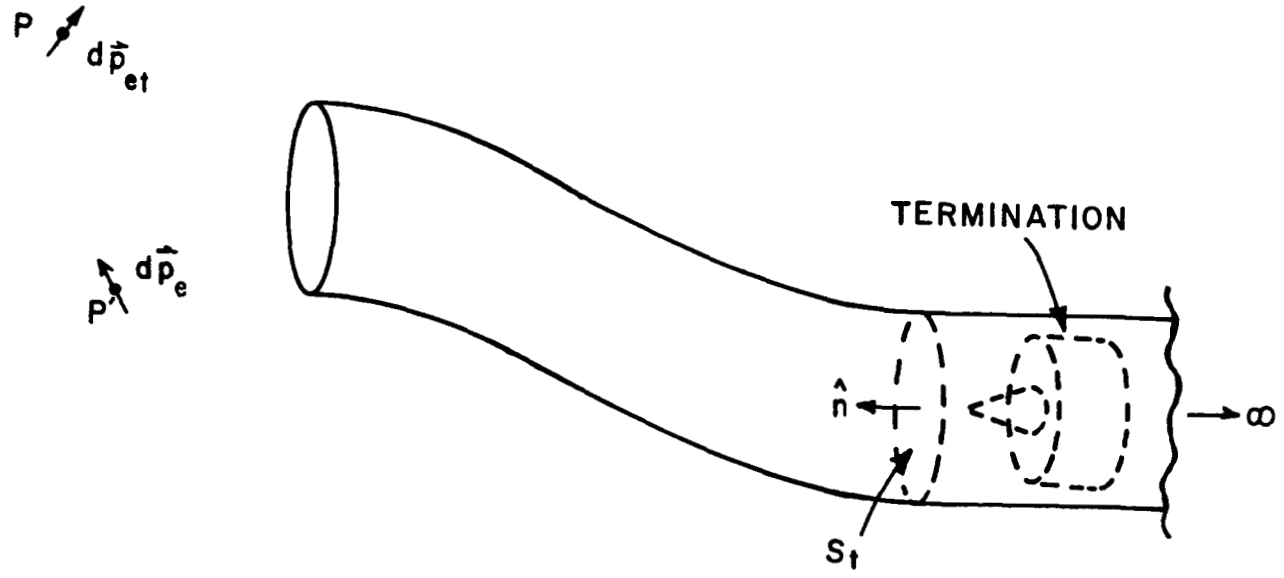

Figure B.1: Open ended waveguide cavity illuminated by two electric dipole sources.

$d\vec{p}_{et}$ evaluated in the presence of the waveguide but in the absence of the termination. $\vec{E}_e^{so}$ and $\vec{H}_e^{so}$ are the fields generated by $d\vec{p}_e$ and scattered by the termination, evaluated in the presence of the waveguide walls, i.e., they are the fields generated by $d\vec{p}_e$ which are reflected by the waveguide termination. The total fields generated by $d\vec{p}_e$ could therefore be written as $\vec{E}_e = \vec{E}_e^{ig} + \vec{E}_e^{so}$ and $\vec{H}_e = \vec{H}_e^{ig} + \vec{H}_e^{so}$ where $\vec{E}_e^{ig}$ and $\vec{H}_e^{ig}$ are the incident fields generated by $d\vec{p}_e$ evaluated in the presence of the waveguide walls but in the absence of the termination.

It should be mentioned that the scattered field of (B.1) does not include the scattering by the open end of the waveguide. This component of the scattered field can be added in separately using a method such as the Geometrical Theory of Diffraction (GTD). Also, (B.1) does not include any multiple interactions between the termination and the open end of the waveguide cavity. However, this effect is usually negligable but it can be included, if desired, with some difficulty.

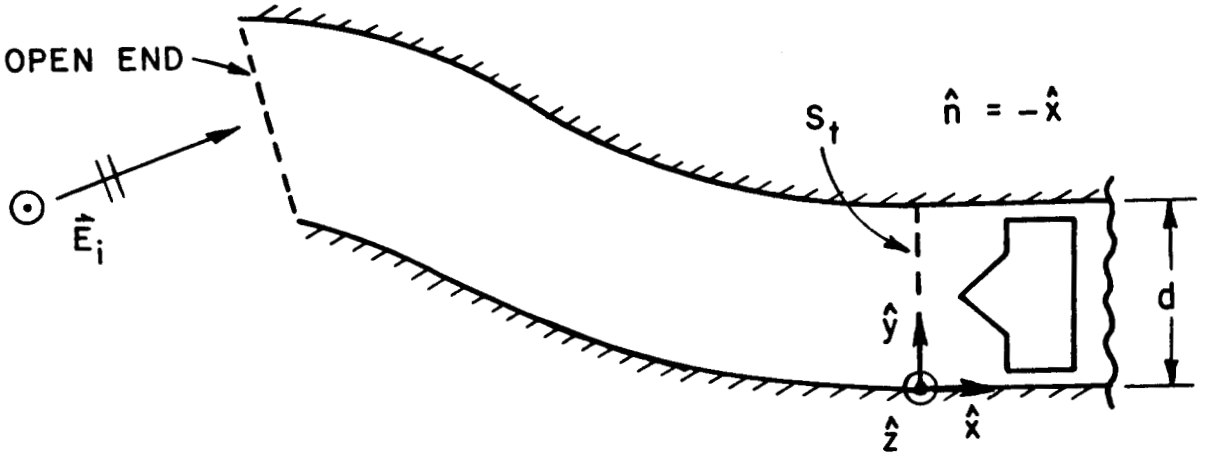

Figure B.2: 2-D open-ended waveguide cavity illuminated by plane wave.

B.2 Reaction Integral for Two Dimensions

The termination reaction integral (B.1) reduces for two dimensional (2-D) configurations, such as the one shown in Figure B.2. This waveguide cavity is illuminated by a plane wave with the E-field in the $\hat{z}$ direction. For this polarization, $\vec{E}$ will always be in the $\hat{z}$ direction. "E" refers to "the scalar portion of $\vec{E}$", or equivalently, $\vec{E} = \hat{z}E$. To obtain the far field scattering due to plane wave illumination using the reaction integral of (B.1), the points P and P' of Figure B.1 are placed a very large distance ρ from the cavity. For the 2-D case, the dipole sources are replaced by z-directed electric line sources of strength I. The left side of (B.1) becomes

$$\begin{aligned} \vec{E}_e^{so}(P) \cdot d\vec{p}_{et} &= [\hat{z}E_e^{so}(P)] \cdot (\hat{z}I) \\ &= E_e^{so}(P)I. \end{aligned} \tag{B.2}$$

The field incident on the open end of the cavity due to an electric line source of strength I located at point P' in the far field is given by

$$\vec{E}_i = \hat{z}E_i \tag{B.3}$$

$$E_i = -Z_o I \sqrt{\frac{jk}{8\pi}} \frac{e^{-jk\rho}}{\sqrt{\rho}} \tag{B.4}$$

where ρ is the distance from the line source and Z_o is the free space impedance of approximately 377 ohms. Substituting for I using (B.4) and rearranging (B.2) gives

$$\begin{aligned} E_e^{so}(P) &= -\frac{Z_o}{E_i} \sqrt{\frac{jk}{8\pi}} \frac{e^{-jk\rho}}{\sqrt{\rho}} \vec{E}_e^{so}(P) \cdot d\vec{p}_{et} \\ &= -\frac{Z_o}{E_i} \sqrt{\frac{jk}{8\pi}} \frac{e^{-jk\rho}}{\sqrt{\rho}} \int\int_{S_a} \left(\vec{E}_t^{ig} \times \vec{H}_e^{so} - \vec{E}_e^{so} \times \vec{H}_t^{ig} \right) \cdot \hat{n} dS \end{aligned} \tag{B.5}$$

The integral of (B.5) simplifies by using one of Maxwell's equations to eliminate the magnetic fields, $\vec{H}_e^{so}$ and $\vec{H}_t^{ig}$. An arbitrary time harmonic magnetic field in a source free region given in terms of a z-directed electric field is

$$\begin{aligned} \vec{H} &= -\frac{1}{jkZ_o} \nabla \times \vec{E} \\ &= -\frac{1}{jkZ_o} \left(\hat{x} \frac{\partial}{\partial x} + \hat{y} \frac{\partial}{\partial y} \right) \times (\hat{z} E) \\ &= \frac{1}{jkZ_o} \left(\hat{y} \frac{\partial E}{\partial x} - \hat{x} \frac{\partial E}{\partial y} \right). \end{aligned} \tag{B.6}$$

The integrand in (B.5) can now be rewritten in terms of the E-field as

$$\begin{aligned} \left(\vec{E}_t^{ig} \times \vec{H}_e^{so} - \vec{E}_e^{so} \times \vec{H}_t^{ig} \right) \cdot \hat{n} &= \left[(\hat{z} E_t^{ig}) \times \frac{1}{jkZ_o} \left(\hat{y} \frac{\partial E_e^{so}}{\partial x} - \hat{x} \frac{\partial E_e^{so}}{\partial y} \right) \right. \\ &\quad \left. -(\hat{z} E_e^{so}) \times \frac{1}{jkZ_o} \left(\hat{y} \frac{\partial E_t^{ig}}{\partial x} - \hat{x} \frac{\partial E_t^{ig}}{\partial y} \right) \right] \cdot (-\hat{x}) \\ &= \frac{1}{jkZ_o} \left(E_t^{ig} \frac{\partial E_e^{so}}{\partial x} - E_e^{so} \frac{\partial E_t^{ig}}{\partial x} \right). \end{aligned} \tag{B.7}$$

With the two dimensional integration over S_a replaced with a one dimensional integration in the y direction and the result of (B.7), (B.5) simplifies to

$$E_e^{so}(P) = -\frac{1}{E_i \sqrt{j8\pi k}} \frac{e^{-jk\rho}}{\sqrt{\rho}} \int_0^d \left(E_t^{ig} \frac{\partial E_e^{so}}{\partial x} - E_e^{so} \frac{\partial E_t^{ig}}{\partial x} \right) dy. \tag{B.8}$$

Replacing E by H in (B.8), by duality the scattered magnetic field for the other polarization is similarly given by

$$H_e^{so}(P) = -\frac{1}{H_i\sqrt{j8\pi k}}\frac{e^{-jk\rho}}{\sqrt{\rho}}\int_0^d \left(H_t^{ig}\frac{\partial H_e^{so}}{\partial x} - H_e^{so}\frac{\partial H_t^{ig}}{\partial x}\right) dy. \quad \text{(B.9)}$$

In (B.8) and (B.9), $E_e^{so}(P)$ and $H_e^{so}(P)$ are the scattered fields at point P due to a plane wave incident on the open end of the waveguide cavity from the direction of P'. E_t^{ig} and H_t^{ig} are the fields due to a plane wave incident on the open end of the cavity from the direction of P in the absence of the termination, and E_e^{so} and H_e^{so} are the fields scattered by the termination due to a plane wave incident on the open end of the cavity from the direction of P'. The incident plane waves are of magnitude E_i or H_i, depending on polarization. In simple terms, the bistatic scattering from the open-ended waveguide cavity is found by tracking the fields coupled into the cavity due to plane waves coming from the source and receiver directions, to a cross-section near the termination. Here, the cross product of the fields from the receiver direction in the absence of the termination and the fields from the source direction scattered by the termination are integrated to give the scattered field at P.

For the simple case of a short circuit termination (i.e., a perfectly conducting planar termination coinciding with S_a), the scattered fields can be written in terms of the incident fields at the termination as

$$E_e^{so} = -E_e^{ig} \quad \text{(B.10)}$$

$$\frac{\partial E_e^{so}}{\partial x} = \frac{\partial E_e^{ig}}{\partial x} \quad \text{(B.11)}$$

$$H_e^{so} = H_e^{ig} \quad \text{(B.12)}$$

$$\frac{\partial H_e^{so}}{\partial x} = -\frac{\partial H_e^{ig}}{\partial x}. \quad \text{(B.13)}$$

(B.8) and (B.9) become

$$E_e^{so}(P) = -\frac{1}{E_i\sqrt{j8\pi k}}\frac{e^{-jk\rho}}{\sqrt{\rho}}\int_0^d \left(E_t^{ig}\frac{\partial E_e^{ig}}{\partial x} + E_e^{ig}\frac{\partial E_t^{ig}}{\partial x}\right) dy \quad \text{(B.14)}$$

$$H_e^{so}(P) = \frac{1}{H_i\sqrt{j8\pi k}}\frac{e^{-jk\rho}}{\sqrt{\rho}}\int_0^d \left(H_t^{ig}\frac{\partial H_e^{ig}}{\partial x} + H_e^{ig}\frac{\partial H_t^{ig}}{\partial x}\right) dy \quad \text{(B.15)}$$

for the short circuit case, where E_e^{ig} and H_e^{ig} are the fields due to a plane wave incident on the open end of the cavity from the direction of the source, and E_t^{ig} and H_t^{ig} are the fields due to a plane wave incident on the open end of the cavity from the direction of the receiver, in the absence of the termination.

For the simple case of backscatter from a cavity with a short circuit termination (i.e., a perfectly conducting planar termination coinciding with S_a), E_e^{ig} and H_e^{ig} become E_t^{ig} and H_t^{ig}, respectively. This reduces (B.14) and (B.15) to

$$E_e^{so} = -\frac{2}{E_i\sqrt{j8\pi k}}\frac{e^{-jk\rho}}{\sqrt{\rho}}\int_0^d E_t^{ig}\frac{\partial E_t^{ig}}{\partial x}dy \tag{B.16}$$

$$H_e^{so} = \frac{2}{H_i\sqrt{j8\pi k}}\frac{e^{-jk\rho}}{\sqrt{\rho}}\int_0^d H_t^{ig}\frac{\partial H_t^{ig}}{\partial x}dy, \tag{B.17}$$

respectively. These last two equations are useful computationally because they are functions of only the incident fields at the termination due to a plane wave incident from the source/receiver direction, in the absence of the termination.

Bibliography

[1] R. Mittra and S.W. Lee, Analytical Techniques in the Theory of Guided Waves, The Macmillan Company, New York, 1971.

[2] P.H. Pathak, C.W. Chuang and M.C. Liang, "Inlet Modeling Studies," The Ohio State University ElectroScience Laboratory Technical Report 717674-1, prepared under Contract No. N60530-85-C-0249, for Naval Weapons Center, China Lake, California, October 1986.

[3] A. Altintas, P.H. Pathak, W.D. Burnside, "Electromagnetic Scattering from a Class of Open-Ended Waveguide Discontinuities," The Ohio State University ElectroScience Laboratory Technical Report 716148-9, prepared under Grant No. NSG-1613, for NASA/Langley Research Center, Hampton, Virginia, March 1986.

[4] R.J. Burkholder, C.W. Chuang, and P.H. Pathak, "Electromagnetic Fields Backscattered from an S-Shaped Inlet Cavity with an Absorber Coating on its Inner Walls," The Ohio State University ElectroScience Laboratory Final Report No. 715723-2, prepared under Grant NAG 3-476, for NASA/Lewis Research Center, Cleveland, Ohio, July 30, 1987.

[5] J.B. Keller, "Geometrical Theory of Diffraction," J. Opt. Soc. Am., Vol. 52, pp. 116-130, 1962.

[6] R.G. Kouyoumjian and P.H. Pathak, "A Uniform Geometrical Theory of Diffraction for an Edge in a Perfectly Conducting Surface," Proc. IEEE, Vol. 62, pp. 1448-1461, November 1974.

[7] P.H. Pathak, "Techniques for High Frequency Problems," Chapter 4 in ANTENNA HANDBOOK - Theory, Applications, and Design, eds.

Y.T. Lo and S.W. Lee, Van Nostrand Reinhold, 1988.

[8] W.D. Burnside and L. Peters, Jr., "Axial RCS of Finite Cones by the Equivalent Current Concept with Higher Order Diffraction," Radio Science, Vol. 7, No. 10, pp. 943-948, October 1972.

[9] P.Ya. Ufimtsev, "Method of Edge Waves in the Physical Theory of Diffraction," (from the Russian "Method Krayevykh voin v fizicheskoy teoril difraktsii," Izd-Vo Sov. Radio, pp. 1-243 (1962), translation prepared by the U.S. Air Force Foreign Technology Division, Wright-Patterson Air Force Base, Ohio; released for public distribution September 7, 1971.

[10] S.W. Lee, "Comparison of Uniform Asymptotic Theory and Ufimtsev's Theory of EM Edge Diffraction," IEEE Trans. on Antennas and Propagation, Vol. AP-25, No. 2, pp. 162-170, March 1977.

[11] A. Altintas, P.H. Pathak, and M.C. Liang, "A Selective Modal Scheme for the Analysis of EM Coupling into or Radiation from Large Open-Ended Waveguides," Trans. on Antennas and Propagation, Vol. 36, No. 1, pp. 84-96, January 1988.

[12] P.H. Law, R.J. Burkholder and P.H. Pathak, "A Hybrid Asymptotic-Modal Analysis of the EM Scattering by an Open-Ended S-Shaped Rectangular Waveguide Cavity," The Ohio State University ElectroScience Laboratory Technical Report No. 719630-2, prepared under Grant NAG 3-476, for NASA/Lewis Research Center, Cleveland, Ohio, December 1988.

[13] R.J. Burkholder, "Backscatter Analysis of Two Conducting Inlets," Master's Thesis, The Ohio State University, Department of Electrical Engineering, Columbus, Ohio, August 1985.

[14] N.H. Myung and P.H. Pathak, "A High Frequency Analysis of Electromagnetic Plane Wave Scattering by perfectly-conducting Semi- Infinite Parallel Plate and Rectangular Waveguides with Absorber Coated Inner Walls," The Ohio State University ElectroScience Laboratory Technical Report 715723-1, prepared under Grant NSG 3- 476, for NASA/Lewis Research Center, Cleveland, Ohio, September 1986.

[15] R. Chou, H. Ling and S.W. Lee, "Reduction of the Radar Cross Section of Arbitrarily Shaped Cavity Structures," Electromagnetics Laboratory Report No. 87-6, prepared under support of NASA/Lewis Research Center, Cleveland, Ohio under Contract NAG3-475 and by the NSF under Contract ECS 83-11345, August 1987.

[16] H. Ling, R. Chou and S.W. Lee, "Shooting and Bouncing Rays: Calculating RCS of an Arbitrary Cavity," 1986 AP-S International Symposium Digest, pp. 293-296, Philadelphia, PA, June 1986. To appear in IEEE Trans. on Antennas and Propagation, January 1989.

[17] H. Ling and R. Chou, "A Versatile Reflector Antenna Pattern Computation Method: Shooting and Bouncing Rays," Microwave and Optical Technology Letters, Vol. 1, pp. 81-87, 1988.

[18] H. Shirai and L.B. Felsen, "Rays, Modes and Beams for Plane Wave Coupling into a Wide Open-Ended Parallel-Plane Waveguide," Wave Motion, Vol. 9, pp. 301-317, 1987.

[19] H. Shirai and L.B. Felsen, "Rays and Modes for Plane Wave Coupling into a Large Open-Ended Circular Waveguide," Wave Motion, Vol. 9, pp. 461-482, 1987.

[20] L.B. Felsen and S.Y. Shin, "Rays, Beams, and Modes Pertaining to the Excitation of Dielectric Waveguides," IEEE Trans. on Microwave Theory and Techniques, Vol. MTT-23, No. 1, pp. 150-161, January 1975.

[21] J.J. Maciel and L.B. Felsen, "Systematic Study of Fields Due to Extended Apertures by Gaussian Beam Discretization," submitted to IEEE Trans. on Antennas and Propagation.

[22] J.J. Maciel and L.B. Felsen, "Gaussian beam analysis of propagation from an extended plane aperture distribution through plane and curved dielectric layers," submitted to to IEEE Trans. on Antennas and Propagation.

[23] P.H. Pathak, R.J. Burkholder, Internal memorandum on the use of a generalized reciprocity theorem to deal with the scattering by an

arbitrary termination within an otherwise open-ended cavity, 1988. A paper describing this work is in preparation.

[24] D. Gabor, "Theory of Communication," J. Inst. Elec. Eng. (London) 93III, 429-457 (1946).

[25] M.J. Bastiaans, "Gabor's Expansion of a Signal into Gaussian Elementray Signals," Proc. IEEE 68, 538-539 (1980).

[26] G.A. Deshamps, "The Gaussian Beam as a Bundle of Complex Rays", Electronics Letters, Vol. 7, No. 23, pp. 684-685, Nov. 18, 1971.

[27] J.W. Ra, H.L. Bertoni, and L.B. Felsen, "Reflection and Transmission of Beams at a Dielectric Interface", SIAM J. Appl. Math., Vol. 24, No.3, pp. 396-413, May 1973.

[28] Y.Z. Ruan and L.B. Felsen, "Reflection and Transmission of Beams at a Curved Interface," J. Optical Society of America, Vol. 3, No. 4, pp. 566-578, April 1986.

[29] F.J.V. Hasselmann and L.B. Felsen, "Asymptotic Analysis of Parabolic Reflector Antennas", IEEE Trans. on Antennas and Propagation, Vol. AP-30, No. 4, pp. 677-685, July 1982.

[30] S.Y. Shin and L.B. Felsen, "Multiply Reflected Gaussian Beams in a Circular Cross Section", IEEE Trans. on Microwave Theory and Techniques, Vol. MTT-26, No. 11, pp. 845-851, November 1978.